

# Modeling the structure of the StART domains of MLN64 and StAR proteins in complex with cholesterol<sup>1,§</sup>

Marta Murcia,\* José D. Faraldo-Gómez,<sup>†</sup> Frederick R. Maxfield,<sup>§</sup> and Benoît Roux<sup>2,†</sup>

Department of Physiology and Biophysics\* and Department of Biochemistry,<sup>§</sup> Weill Medical College of Cornell University, New York, NY 10021; and Department of Biochemistry and Molecular Biology and Institute for Molecular Pediatric Sciences, Center for Integrative Sciences,<sup>†</sup> University of Chicago, Chicago IL 60637

**Abstract** Steroidogenic acute regulatory protein-related lipid transfer (StART) domains are ubiquitously involved in intracellular lipid transport and metabolism and other cell-signaling events. In this work, we use a flexible docking algorithm, comparative modeling, and molecular dynamics (MD) simulations to generate plausible three-dimensional atomic models of the StART domains of human metastatic lymph node 64 (MLN64) and steroidogenic acute regulatory protein (StAR) proteins in complex with cholesterol. Our results show that cholesterol can adopt a similar conformation in the binding cavity in both cases and that the main contribution to the protein-ligand interaction energy derives from hydrophobic contacts. However, hydrogen-bonding and water-mediated interactions appear to be important in the fine-tuning of the binding affinity and the position of the ligand. To gain insights into the mechanism of binding, we carried out steered MD simulations in which cholesterol was gradually extracted from within the StAR model. These simulations indicate that a transient opening of loop  $\Omega 1$  may be sufficient for uptake and release, and they also reveal a pathway of intermediate states involving residues known to be crucial for StAR activity. **Based on these observations, we suggest specific mutagenesis targets for binding studies of cholesterol and its derivatives that could improve our understanding of the structural determinants for ligand binding by sterol carrier proteins.**—Murcia, M., J. D. Faraldo-Gómez, F. R. Maxfield, and B. Roux. **Modeling the structure of the StART domains of MLN64 and StAR proteins in complex with cholesterol.** *J. Lipid Res.* 2006. 47: 2614–2630.

**Supplementary key words** steroidogenic acute regulatory protein • steroidogenic acute regulatory protein-related lipid transfer • metastatic lymph node 64 • docking • homology modeling • generalized-Born • binding • molecular dynamics • steered molecular dynamics • cholesterol release

Steroid hormones play a critical role in a wide range of biological processes in mammals, such as sexual development and reproduction, neurogenesis and synaptic plasticity, and homeostasis and tumor growth (1, 2). In all

cases, hormone biosynthesis begins with the conversion of cholesterol to pregnenolone on the matrix side of the inner mitochondrial membrane. The steroidogenic acute regulatory protein (StAR) facilitates both the mobilization of cholesterol from multiple sources to the outer mitochondrial membrane and its subsequent translocation to the inner mitochondrial membrane (3, 4). StAR-mediated delivery of cholesterol is in fact the rate-limiting step of steroidogenesis and thus is strongly regulated (5, 6). Because other types of cholesterol transporters, such as the sterol carrier protein-2, cannot replace StAR (7), a number of developmental and reproductive abnormalities in humans are related to the misregulation of StAR expression and/or to a nonfunctioning StAR gene (8). For instance, more than 34 different congenital mutations are known to produce nonfunctional StAR proteins (9–11), which lead to a potentially lethal autosomal recessive disease known as congenital lipoid adrenal hyperplasia (12–14).

StAR is a 285 amino acid protein with two major domains (5, 15): first, an N-terminal targeting sequence nonessential to its activity that is cleaved upon entry into the mitochondria (16–18); second, a 30 kDa C-terminal domain (200–210 residues), known as the steroidogenic acute regulatory protein-related lipid transfer (StART) domain (19), which is the domain that binds cholesterol (7, 20). The StART domain of the StAR protein (referred to hereafter as StAR-StART) is also the prototype of a larger, only partially characterized family of lipid binding domains found in other eukaryotic proteins, which are essential in a variety of important processes such as lipid transport and metabolism and cell signaling (3). Various StART domain proteins may play a more widespread role as cholesterol carriers in the nonvesicular transport of

<sup>1</sup>Coordinates of both MLN64- and StAR-StART domains in complex with cholesterol have been deposited in the Protein Data Bank (accession code 2I92 and 2I93 respectively).

<sup>2</sup>To whom correspondence should be addressed.  
e-mail: roux@uchicago.edu

§ The online version of this article (available at <http://www.jlr.org>) contains supplemental data in the form of movies and seven figures.

Manuscript received 30 May 2006 and in revised form 18 September 2006.  
Published, JLR Papers in Press, September 21, 2006.  
DOI 10.1194/jlr.M600232-JLR200

Copyright © 2006 by the American Society for Biochemistry and Molecular Biology, Inc.

cholesterol between cellular organelles through the cytoplasm (21). Putative StART domain proteins have also been described in bacteria and unicellular protists (22). StART domains are distinct from other known lipid-transfer proteins and are believed to be highly specific for their ligands, which include cholesterol, phosphatidylcholine (PC), carotenoid, and ceramide (23, 24), although a common ligand binding mechanism is thought to be characteristic of the entire StART superfamily (25).

Fifteen StART domain proteins have been identified to date in humans (3, 23). Among these, the closest homolog to that in StAR is the C-terminal domain of a two-domain protein known as metastatic lymph node 64 (MLN64), which also binds cholesterol (20) and which is overexpressed in certain breast cancers. MLN64 is a 445-residue protein anchored to the late endosome membrane through its N-terminal domain (26). Its function is thought to be the export of cholesterol through its cytosolic StART domain, which resembles somewhat the mitochondrial action of StAR (27, 28). The StART domain of MLN64 (MLN64-StART) is able to stimulate steroidogenesis in human placentas, which generally lack StAR (29). In addition, several specificity-related residue patterns as well as many of the pathological mutations of human StAR-StART are also found in MLN64-StART, but not in other members of the family.

Although the atomic structure of the StAR-StART domain remains unknown, those of three related StART domains have been determined by X-ray crystallography, namely human MLN64 (20), mouse StarD4 (30), and human phosphatidylcholine transfer protein (PCTP) (31). Of these, only PCTP has been resolved with its ligand bound inside the cavity. More recently, the structures of bacterial members of the StART superfamily of unknown specificity have also been solved in the *apo* state by means of NMR spectroscopy (32) or crystallography (33). Finally, ligand-free and -bound structures of the phosphatidylinositol transfer protein  $\alpha$  (PITP $\alpha$ ), whose architecture and function are comparable to those of StART, are also known. All of these binding domains share a common "helix-grip" fold, with a characteristic hydrophobic cavity, formed by  $\beta$ -strands, where the ligand binds. Access into this cavity is occluded by the domain's C-terminal  $\alpha$ -helix and by adjacent loops. Conformational changes in these, presumably upon the domain's association with a membrane, are believed to enable ligand uptake or release (23). Consistently, several disease-related mutations or truncations in human StAR appear to correspond to residues lining the interior of the hydrophobic cavity, or in the C-terminal  $\alpha$ -helix, when mapped onto the MLN64-StART structure (13, 18, 34).

The potential role of StART domains as drug targets has prompted an increasing interest in their function, especially in the case of the prototypical StAR protein. Nonetheless, a detailed structural understanding of their binding properties is still lacking, in part because of inherent experimental difficulties associated with these systems. In this work, we use computational methods to gain insights into the association of two StART domains with their cholesterol ligand. Specifically, we use docking and homology modeling algorithms, as well as molecular

dynamics (MD) simulations, to generate plausible three-dimensional atomic models of both MLN64-StART and StAR-StART domains in complex with cholesterol. Through these and additional simulations, in which cholesterol is gradually extracted from the binding site within these domains, we hope to provide specific clues for future analyses of the mechanism of uptake and release as well as for the interpretation or design of experimental work focusing on other cholesterol derivatives in the more general context of sterol carrier proteins.

## METHODS

### Overview

The computational protocol presented here can be divided into three parts. First, an exhaustive docking study of cholesterol binding in the cavity of MLN64-StART was carried out to identify and classify the possible binding modes that cholesterol may adopt in the MLN64 cavity. MD simulations were subsequently used to more thoroughly sample conformations of the protein-ligand complex in each binding mode as well as to derive a more reliable ranking of the binding energies. Second, having determined the most favored binding mode for MLN64-StART, a homology model of the StAR-StART domain in complex with cholesterol was built using the MLN64 complex as a template and further analyzed through MD simulations. Finally, steered MD simulations were carried out to gain insights into the process of uptake and release of cholesterol.

All MD simulations were performed using version c31a0 of the CHARMM biomolecular simulation software (35) alongside the CHARMM22/CMAP all-atom protein force field (36). The cholesterol parameters correspond to the CHARMM27 force field released with version c32a1 of CHARMM (37). An implicit model of the solvent was used in all simulations, as implemented in the GBSW module of CHARMM (38). Atomic radii were those derived by Nina, Im, and Roux (39), and no cutoff was used for the nonbonded interactions or the GBSW terms. The dielectric constants of the protein and solvent were  $\epsilon_p = 1$  and  $\epsilon_s = 80$ , respectively. The nonpolar surface tension coefficient  $\gamma$  was set to 0.025 kcal/mol/Å<sup>2</sup>. All simulations included a Langevin heat bath at 300 K, unless stated otherwise. Bond lengths involving hydrogen atoms were constrained using SHAKE (40).

### Docking cholesterol into the cavity of MLN64-StART

The atomic coordinates of MLN64-StART were obtained from the 2.2 Å-resolution crystal structure (1em2) (20), as deposited in the Protein Data Bank (41–43). Although this structure includes a methionine substitution at position phenylalanine 388, biochemical analyses have demonstrated that this mutant form is competent for binding cholesterol (20). Hydrogen atoms were added using HBUILD within the CHARMM package, and their positions were refined by energy minimization. Initial atomic coordinates for cholesterol were obtained from the crystal structure of the binding domain of the retinoic acid receptor related-orphan nuclear hormone receptor  $\alpha$  (ROR $\alpha$ ) (1n83; 1.63 Å resolution) (44).

The automated docking protocol Flexdock (45) was used for the initial screening of the binding poses of cholesterol into the MLN64-StART cavity. This algorithm carries out an exhaustive translational and rotational search of the ligand within the binding site while considering the protein to be rigid. To account for the flexibility of the ligand, the protocol takes into account its

torsional degrees of freedom, which are discretized into coarse rotameric states; in this case, a library of 69 rotamers was generated. To partially account for the protein flexibility, an ensemble of 100 protein conformations of MLN64-StART was generated by means of a 1 ns MD simulation at 500 K, in which the protein's backbone remained harmonically restrained. After energy minimization, the ensemble-averaged root mean square deviation (RMSD) relative to the crystallographic structure was  $0.192 \pm 0.002$  Å for the nonhydrogen atoms in the backbone and  $1.6 \pm 0.1$  Å for those in the side chains. The cholesterol rotamer library mentioned above was docked on each of the protein conformations and the resulting complexes scored as described elsewhere (45). The 20 best-scored solutions for each protein conformation were selected for further analysis, giving a total of 2,000 poses.

### Clustering analysis of the cholesterol binding modes obtained after docking

To analyze the ensemble of solutions and extract representative configurations, we considered two clustering order parameters. First, we used the pseudo-dihedral angle defined by the  $\alpha$  carbons of arginine 351 (Arg351) and glutamine 421 (Gln421) in MLN64-StART, and two carbon atoms in the cholesterol ring (C3 and C17), which roughly describes the orientation of the long axis of the ligand relative to the hydrophobic cavity. Second, we carried out an average-linkage hierarchical clustering based on the pair-wise RMSD of the ring moiety of cholesterol, using CLUSBAS (46), to further characterize the position and orientation of the ligand in the binding site.

### MD simulations of the MLN64-cholesterol complexes

The best-scored pose of each of the four selected clusters was energy-minimized and further analyzed by means of multiple MD simulations. Specifically, we carried out 10 independent simulations of 1.5 ns for each configuration of the MLN64-StART complex, over which results are averaged. In terms of the potential energy and the RMSD values of the structure of the protein-cholesterol complex, all simulations appeared to be equilibrated within 1 ns. The analysis reported below corresponds to the last 500 ps fragment of each trajectory.

### Scoring of the cholesterol binding modes

To identify the most favorable binding mode, an ensemble of 1,000 configurations of the protein-ligand complex was extracted from the last 500 ps fragment of each simulation, and the corresponding binding free energy,  $\Delta G_b$ , was estimated according to the expression  $\Delta G_b = \langle \Delta U_{\text{inter}} \rangle + \Delta G_s^{(\text{complex})} - \Delta G_s^{(\text{protein})} - \Delta G_s^{(\text{ligand})}$ , where  $\langle \Delta U_{\text{inter}} \rangle$  is the average interaction energy between the ligand and the protein ( $\Delta U_{\text{inter}} = \Delta U_{\text{VDW}} + \Delta U_{\text{elec}}$ ) and  $\Delta G_s^{(\text{complex})}$ ,  $\Delta G_s^{(\text{protein})}$ , and  $\Delta G_s^{(\text{ligand})}$  are the solvation free energies of the complex, protein, and ligand, respectively (all bonded terms cancel out under this approximation). The solvation free energies can in turn be separated into a nonpolar contribution,  $\Delta G_{s,\text{np}}$ , and an electrostatic contribution,  $\Delta G_{s,\text{elec}}$  (47), both of which are included within the generalized-Born formalism used here. The values of  $\Delta G_b$  reported below correspond to averages over the 10 independent simulations that were carried out for each of the hypothetical binding poses of cholesterol.

### Comparative modeling of the StAR-StART domain in complex with cholesterol

A homology model of the three-dimensional structure of human StAR-StART in complex with cholesterol was built with

CHARMM using the MLN64-StART crystal structure as a template, based on a pair-wise sequence alignment produced with ClustalW (48) (see supplementary Figure 1). The identity of both sequences is 36%, with no insertions or deletions. The coordinates of all backbone atoms as well as those of conserved or structurally similar side chains [e.g., aspartate (Asp) and asparagine (Asn)] were preserved from the template. Otherwise, new coordinates were assigned using SCWRL 3.0 (49) and subsequently energy-minimized using a distance-dependent dielectric constant,  $\epsilon = r$  (Å). A cholesterol molecule in the preferred binding mode in MLN64-StART was included while building the model. (Direct docking of cholesterol into a model of StAR built without the ligand, and following the same procedure as for the crystal structure of MLN64-StART, failed to find any poses inside the cavity.) The three-dimensional model of the atomic structure of StAR-StART in complex with cholesterol was finally analyzed through MD simulations as described previously for MLN64-StART.

### Simulation of cholesterol release by steered MD

Starting from the last configuration of two of the simulations of the StAR-StART complex (chosen at random), the release of cholesterol was modeled by MD simulations in which the ligand was gradually extracted from the binding cavity without any directional bias. Specifically, a harmonic potential was applied to the distance between the center of mass of cholesterol and that of the backbone atoms of residues leucine 199 (Leu199) and alanine 200 (Ala200) at the end of the cavity, and the corresponding equilibrium distance was shifted at a rate of  $0.01 \text{ Å ps}^{-1}$  and  $0.02 \text{ Å ps}^{-1}$ . The range of distances explored was 12–40 Å, and two different force constants for the harmonic potential were used in independent simulations:  $2 k_B T \text{ Å}^{-2}$  and  $8 k_B T \text{ Å}^{-2}$ . Analogous simulations were carried out for the MLN64-StART complex, at a rate of  $0.01 \text{ Å ps}^{-1}$  and identical force constants.

## RESULTS AND DISCUSSION

### MLN64-StART in complex with cholesterol

*Docking and identification of possible cholesterol binding modes.* Of the 2,000 best-scored solutions obtained from the docking protocol, a total of 1,357 were found inside the MLN64-StART cavity. The remaining poses, corresponding to configurations in which the ligand docked elsewhere on the protein's surface, were discarded. Two main families of poses were identified after initial clustering of the successful solutions: those in which the cholesterol hydroxyl group points toward the bottom of the cavity, termed hereafter IN (1,030 solutions), and those with a reverse orientation, or OUT (327 solutions). A representation of MLN64-StART with cholesterol bound in an IN configuration is depicted in **Fig. 1**.

Further clustering according to the orientation and position of the cholesterol ring resulted in six subfamilies for both the IN and OUT configurations, all of which are shown in **Fig. 2A**. Analysis of the populations of these subfamilies shows that the scoring function used by the docking algorithm favors poses in two specific orientations of the methyl groups in the cholesterol ring, which are opposite to each other; these will be referred to as IN-1 (868 solutions; cluster 1) and OUT-1 (52 solutions; cluster 5) and IN-2 (94 solutions; cluster 3) and OUT-2



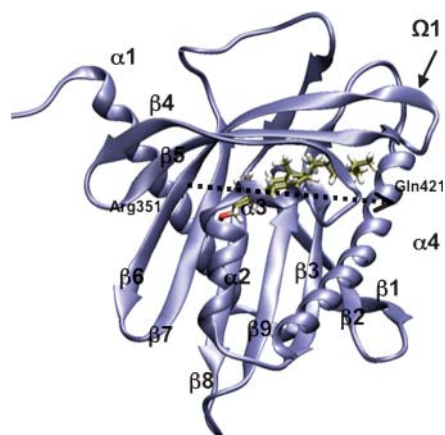


**Fig. 1.** Ribbon representation of the StART domain of the meta-static lymph node 64 protein (MLN64-StART), with cholesterol bound in the IN-1 configuration. VMD (for visual molecular dynamics; 104) was used for all molecular graphics hereafter. The axis used as a descriptor of the orientation of the ligand relative to the cavity (IN/OUT) is indicated.

(195 solutions; cluster 1). Examination of representative poses of the remaining clusters did not reveal significantly different features in the binding mode (Fig. 2A); given their lower populations, we chose to continue our study with the four configurations described above, which are depicted in **Fig. 3**.

A summary of the scoring results for the selected four clusters is given in Fig. 2B. It is worth noting that the scores are dominated by the van der Waals component of the protein-ligand interaction energy and that this contribution is unfavorable on average as a result of steric clashes that result from the docking procedure. This is consistent with the nonpolar nature of the binding cavity and with the fact that the crystal structure of MLN64 corresponds to the ligand-free state. Nonetheless, many of the poses in cluster 1 IN yield a negative value for the interaction energy between the protein and the ligand, in accordance with the rather selective preference of the docking algorithm for this particular binding mode. Given the inherent limitations of the configurational sampling of the protein-ligand complex during the docking procedure, as well as the simplicity of the scoring function, this initial stage serves to screen the possible modes of binding of cholesterol to MLN64-StART. No attempt at further discrimination is made at this point.

*MD simulations of the four hypothetical binding modes.* The four hypothetical binding modes mentioned above were subsequently analyzed through multiple MD simulations (see Methods), up to a total sampling time of 15 ns per mode. The first conclusion from these calculations is that the different binding modes of cholesterol do not result in significantly different deviations in the overall architecture of MLN64-StART relative to the crystal structure. Specifically, the average RMSD of the protein's backbone is 0.7–0.8 Å for the  $\beta$ -strand segments, 1.1–1.0 Å for the helical regions, and 1.2–1.3 Å overall, whereas the RMSD for all

of the nonhydrogen atoms is in the 1.7–1.9 Å range (**Table 1**). Analysis of the per-residue contributions to the backbone RMSD values (see supplementary Fig. II) reveals that the most notable changes occur in the loops at the entrance of the hydrophobic cavity, namely those between strands  $\beta 5$  and  $\beta 6$  (loop  $\Omega 1$ , residues 335–344) and between strands  $\beta 2$  and  $\beta 3$  (residues 277–279), as well as in the region around the N-terminal end of the C-terminal  $\alpha$ -helix (residues 410–425). With regard to the side chains, only Arg351 in the interior of the protein displays noticeable changes with respect to the crystallographic structure ( $\sim 2$  Å).

Although only subtle differences are observed in the protein structure during the simulations, the dynamics of cholesterol in the alternative binding modes are strikingly dissimilar (**Table 2**). In particular, the binding modes least favored by the Flexdock scheme, namely modes IN-2 and OUT-1, yield much larger displacements from the initial conformation than IN-1 and OUT-2, as measured by the RMSD of the nonhydrogen atoms in the cholesterol ring (1.85 and 1.98 Å vs. 0.71 and 0.74 Å, respectively). Comparison of the simulations of the same pose shows that those modes with the lowest RMSD values also display the smallest fluctuations around the average (0.98 and 0.35 vs. 0.08 and 0.15, respectively). Detailed examination of each simulation reveals that in one of the simulations of IN-2 and OUT-1, the cholesterol molecule flips its orientation around the long axis after several hundred picoseconds (**Table 2**; see supplementary Fig. III).

Overall, this analysis indicates that the cavity of the StART domain of MLN64 is well suited for a ligand of the size and shape of cholesterol without significant deviations from the *apo* form. The loops at the entrance of the hydrophobic cavity may display an alternative conformation upon binding. These simulations agree with the docking scoring in that modes IN-1 and OUT-2 are preferred.

*Ranking of binding energies from the simulation ensemble.* To further discriminate among the hypothetical binding poses of cholesterol in MLN64-StART, we derive a ranking of the corresponding binding energies for each of the ensembles generated with MD simulations, as described in Methods. Although this approach is clearly unsuitable for a rigorous calculation of the binding free energy (50–53), it is considered to be adequate enough to identify the most likely binding mode of protein-ligand complexes (54, 55).

As shown in **Table 3**, mode IN-1 yields the most favorable binding energy, although the difference with mode OUT-1 is marginal. In all cases, the largest contribution to the binding energy originates from the van der Waals interaction between ligand and receptor, whereas the favorable electrostatic component is much smaller. This is consistent with the nonpolar nature of both the cavity and the ligand. As expected, the electrostatic contribution to the desolvation energy upon binding opposes the formation of the complex, whereas the nonpolar component, which reflects the decrease in the solvent-accessible surface area, contributes favorably. Both terms roughly cancel

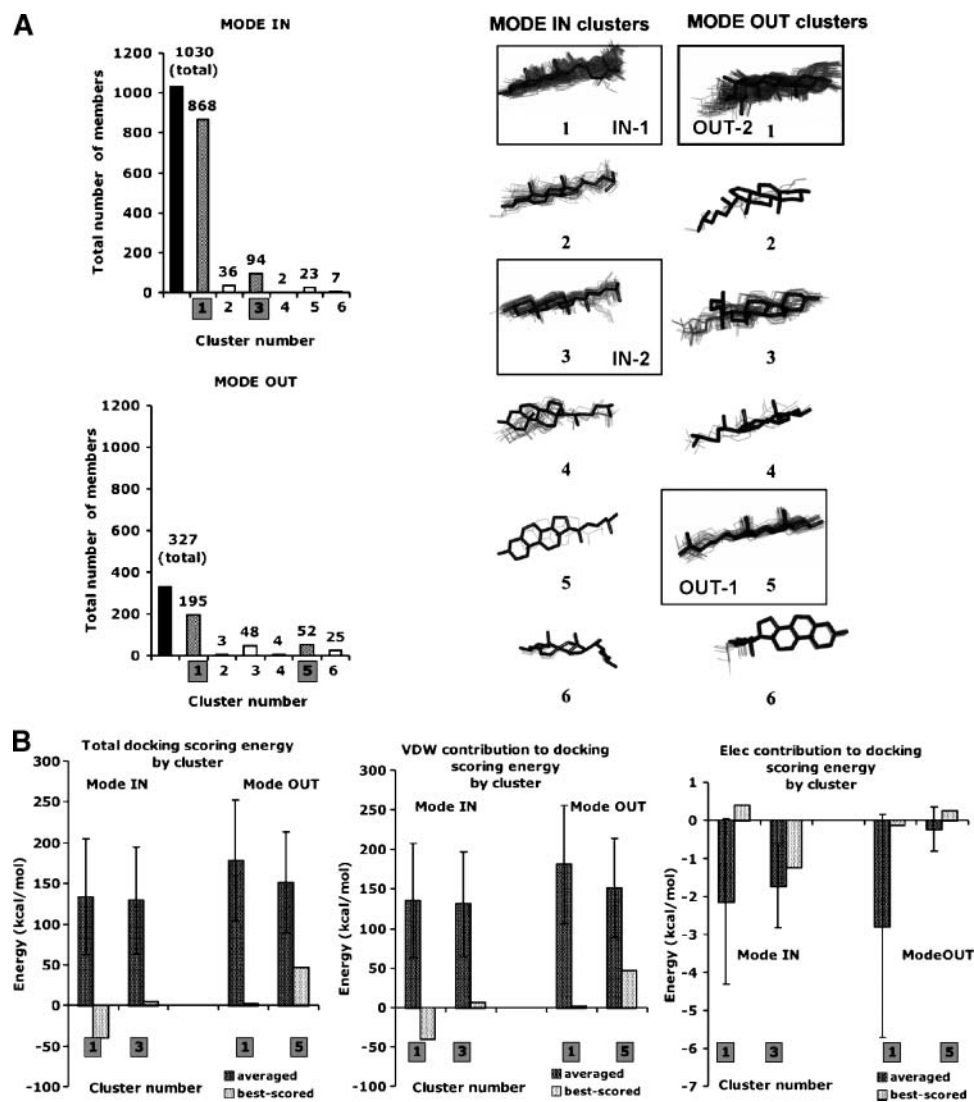


**Fig. 2.** Root mean square deviation (RMSD)-based clustering of the poses derived from docking cholesterol into MLN64-StART. **A:** Population of the different clusters in the IN and OUT configurations, alongside the corresponding structures. The four hypothetical poses selected after clustering for further analysis through molecular dynamics (MD) simulations are shown inside the frames. **B:** Flexdock scoring energy values for the four most populated clusters. Dark gray bars represent average values and their corresponding standard deviations. The energy values for the best-scored members of these clusters are shown with light gray bars.

out and are comparable across modes (within 1 kcal/mol). Therefore, the discrimination between the different binding modes arises from the protein-ligand interaction energy. In particular, among the OUT modes, OUT-1 seems to be favored mainly because of the electrostatic contribution (by  $\sim 2$  kcal/mol). Similarly, the mode IN-1 presents better electrostatics than IN-2 (by  $\sim 3$  kcal/mol), and an additional gain comes from the van der Waals interaction (2.6 kcal/mol). Sampling of the configurations corresponding to mode IN-1 yields very homogeneous values of the binding energy and all its components across the multiple simulations (see values of standard deviation). By contrast, larger differences are observed in mode OUT-1 and notably in modes IN-2 and OUT-2, mainly because of variations in the electrostatic interaction en-

ergy term (Table 3). As will be discussed next, this variability is attributable to alternative protein-ligand contacts.

*Analysis of the cholesterol-protein electrostatic contacts.* The favorable electrostatic contributions observed in the IN-1 and OUT-1 configurations result from stable hydrogen bonds between the hydroxyl group of cholesterol and the protein (Figs. 3, 4). In the IN-1 mode (Fig. 3), cholesterol forms a hydrogen bond at the end of the cavity with both the side chain and the backbone carbonyl of serine 362 (Ser362) (average residence times of 98% and 65% of the simulations, respectively; see Fig. 4). In the case of IN-2 (Fig. 3), although the interaction with the side chain of Ser362 is still possible, the slightly different orientation of the cholesterol ring favors the association of the hydroxylic

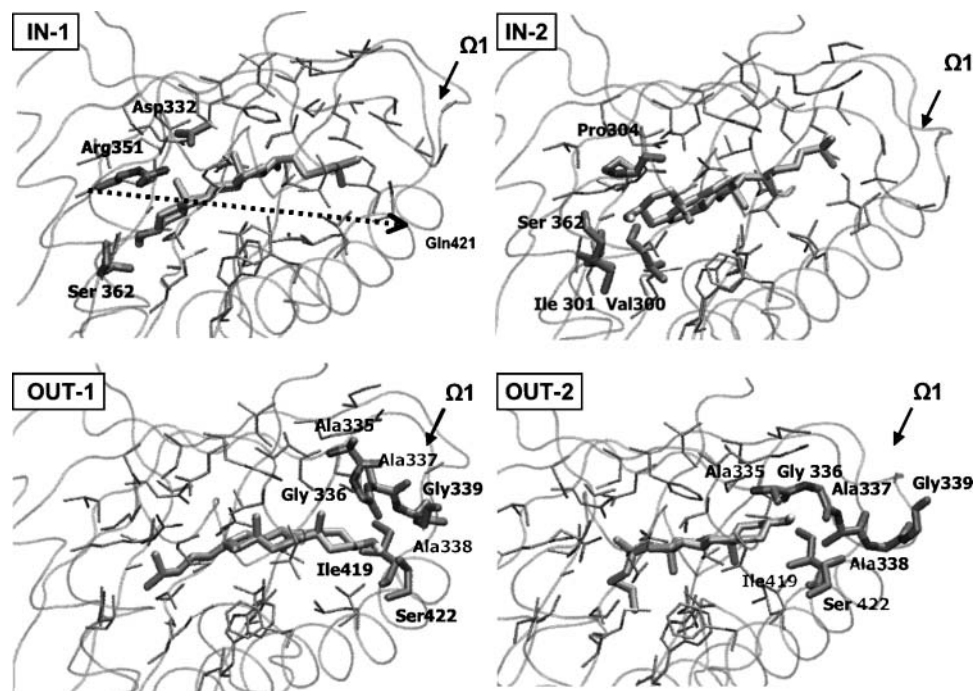


**Fig. 3.** Close-up view of the binding features of the four hypothetical modes for the cholesterol bound to MLN64-StART. A representative configuration of each ensemble is shown.

head also with the backbone carbonyl groups of valine 300 (Val300) or isoleucine 301, or alternatively, with proline 304. However, these contacts have significantly shorter residence times (<41%) than those in IN-1 (Fig. 4) and display more variability across simulations.

In the case of mode OUT-1 (Fig. 3), cholesterol forms hydrogen bonds primarily with the side chain of Ser422 at the N terminus of the C-terminal helix and less frequently with the backbone amide of Ala338 in loop  $\Omega 1$  (average residence times of 76% and 18%, respectively). Thus, the relatively large displacements of the ligand in this binding mode relative to the docking output (Table 2) appear to be concurrent with deviations in the structure of this region of the protein during the simulations (Fig. 3). Finally,

OUT-2 (Fig. 3) displayed only short-lived hydrogen bonds with Ala335 and glycine 336 (Gly336) in loop  $\Omega 1$ , as well as with Ser422 (residence times < 13%).

**Biological insights.** According to the computations, binding modes IN-1 and OUT-1 appear to be equally probable. However, consideration of the biological context of the uptake and release processes leads us to believe that binding of cholesterol to MLN64-StART in a configuration similar to IN-1 is most likely. StART domains have been shown to associate with cholesterol-containing membranes during transport (7, 56, 57), and several lines of evidence indicate that they do so through the C-terminal helix and loops at the entrance of the binding cavity (58).

**TABLE 1.** Ensemble-averaged RMSD values of the MLN64-StART domain for each of the four hypothetical binding modes of cholesterol with respect to the crystal structure

Atoms	IN-1	IN-2	OUT-1	OUT-2
BB	1.3 (0.1)	1.3 (0.1)	1.3 (0.1)	1.2 (0.2)
BB-BETA	0.8 (0.1)	0.8 (0.1)	0.7 (0.1)	0.8 (0.2)
BB-HELIX	1.1 (0.2)	1.1 (0.1)	1.0 (0.1)	1.0 (0.1)
NON-H	1.8 (0.1)	1.9 (0.1)	1.8 (0.1)	1.7 (0.2)

MLN64-StART, StART domain of the metastatic lymph node 64 protein; RMSD, root mean square deviation. The least-square fitting was carried out considering only the  $\beta$ -strand elements of the structures. BB refers to all backbone atoms; BB-BETA and BB-HELIX indicate backbone atoms of the  $\beta$ -strand elements and helical regions, respectively, as assigned with the program STRIDE (105, 106); NON-H refers to all nonhydrogen atoms of the protein. RMSD values are in Å. The standard deviations of the time-averaged RMSD values derived from each of the 10 simulations carried out per binding mode are given in parentheses.

**TABLE 2.** RMSD of the cholesterol ring scaffold (including the two methyl substituents, excluding hydrogen atoms) in the four hypothetical binding modes in the cavity of MLN64-StART with respect to the conformation at the start of the simulation

Simulation No.	IN-1	IN-2	OUT-1	OUT-2
1	0.8	1.7	1.8	0.8
2	0.7	0.7	1.7	0.7
3	0.9	1.2	1.7	1.1
4	0.7	2.0	2.1	0.6
5	0.7	1.0	1.6	0.7
6	0.7	2.0	2.0	0.7
7	0.6	1.0	2.0	0.9
8	0.7	2.3	2.4	0.7
9	0.6	2.6	<b>2.7</b>	0.6
10	0.7	<b>4.0</b>	1.7	0.7
Average	0.7 (0.1)	1.8 (1.0)	2.0 (0.3)	0.7 (0.1)

The computation of the RMSD is analogous that in Table 1. RMS displacement values are in Å. The simulations in which the cholesterol ring flips, with respect to the starting position, are shown in boldface.



TABLE 3. Binding energy values ( $\Delta G_b$ ) for the four analyzed binding poses of cholesterol in the MLN64-StART domain, and the various contributions thereof (see Methods)

Parameter	IN-1	IN-2	OUT-1	OUT-2
$\Delta G_b$	-69.7 (1.0)	-61.7 (3.7)	-68.2 (1.7)	-64.7 (2.8)
$\Delta U_{VDW}$	-56.7 (0.9)	-54.2 (1.6)	-56.2 (0.8)	-56.0 (0.8)
$\Delta U_{elec}$	-11.2 (0.7)	-8.1 (4.4)	-10.6 (2.1)	-8.4 (3.4)
$\Delta \Delta G_{s, np}$	-14.8 (0.2)	-14.2 (0.9)	-15.4 (0.4)	-15.0 (0.1)
$\Delta \Delta G_{s, elec}$	13.0 (0.6)	14.7 (1.7)	14.0 (0.9)	14.6 (0.9)

All values were obtained by first averaging over the 1,000 configurations collected from the last 500 ps of each simulation and binding mode, and subsequently averaging over the 10 independent simulations. Binding energy values are in kcal/mol. The standard deviations of the per-simulation averages are given in parentheses.

The overall positive electrostatic potential in this region of MLN64 is consistent with its association with acidic membranes. Furthermore, by analogy with the mammalian PITP $\alpha$ , whose architecture and function are comparable to those of StART (59–63), these loops are believed to undergo conformational changes that result in the opening of the cavity, thus allowing the translocation of the ligand (26) (see below for further discussion). Superimposition of the structure of MLN64 and PITP $\alpha$ , as shown by Yoder et al. (63), suggests that a common mechanism for the opening of their cavities may exist and that the membrane anchoring and the presentation of the ligand may be similar. Bearing in mind that the orientation of cholesterol in the

membrane is such that its polar head points toward the water-lipid interface (64–66), only binding modes in the IN configuration appear to be mechanistically plausible. Consistent with this argument, the orientation of the PC lipid bound to the crystal structure of the PCTP StART domain is such that its polar head group points toward the end of the binding cavity, and not its entrance (31). The interaction that makes mode OUT-1 comparable in energy to IN-1 would not be available in the putative open state suggested by PITP $\alpha$ . Consequently, we will model the structure of the homologous StART domain of the StAR protein assuming the binding mode IN-1 (Fig. 1).

### StAR-StART in complex with cholesterol

*Modeling and simulations of the StAR-StART domain in complex with cholesterol.* A homology model of the three-dimensional structure of the human StAR-StART in complex with cholesterol was built using the crystal structure of MLN64-StART as template, with cholesterol occupying the binding cavity in the IN-1 mode (Fig. 1). The sequence alignment on which the model is based is shown in supplementary Fig. I.

The model of StAR-StART in complex with cholesterol was subsequently refined by means of multiple MD simulations, as described previously. The backbone RMSD for the resulting ensemble of conformations closely resembles that of the MLN64 template (Table 4), although the structural deviations in these simulations are slightly larger

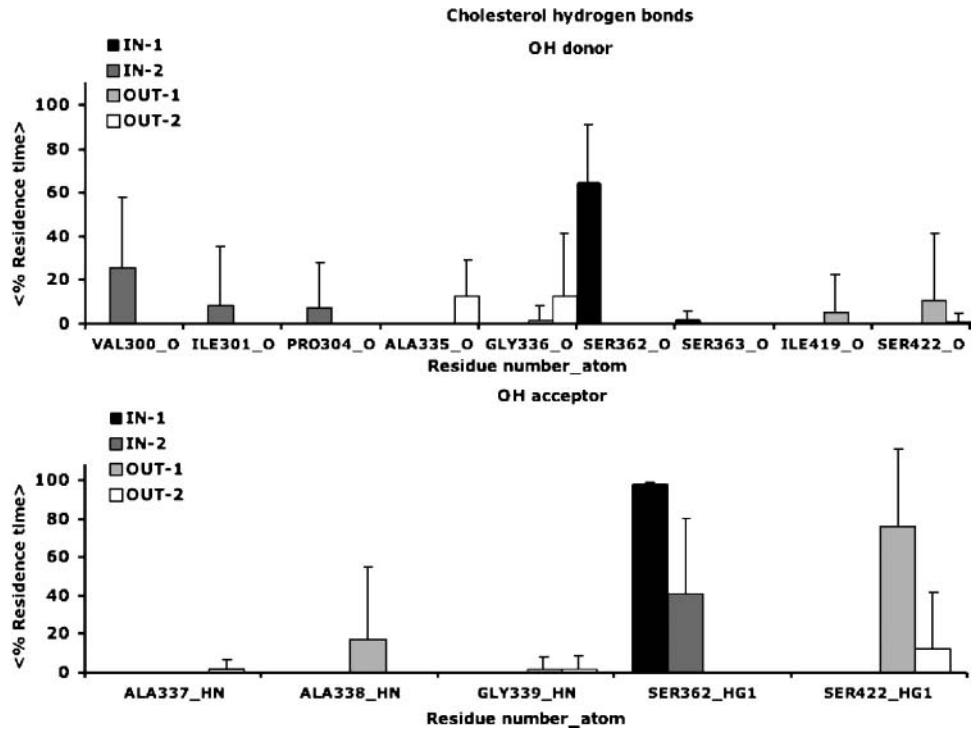


Fig. 4. Hydrogen bonds between MLN64-StART and the hydroxyl group of cholesterol (donor and acceptor) during the simulations of the four hypothetical binding modes, expressed as average percentage residence times (black bars, IN-1; dark gray bars, IN-2; light gray bars, OUT-1; white bars, OUT-2). For a given simulation, the residence time of a hydrogen bond is simply the fraction of the ensemble in which the bond is present. The error bars represent the SD over the simulation in each set.

TABLE 4. Average RMSD values for the protein and the cholesterol ring, computed from the simulations of the model of the StAR-StART/cholesterol complex, alongside the corresponding binding energy and contributions thereof (as in Tables 1–3)

StAR-StART/cholesterol simulations			
Protein RMSD		Cholesterol Ring RMSD	
BB	2.0 (0.2)	Simulation #	Time Average
BB-BETA	1.1 (0.2)	1	2.7
BB-HELIX	2.1 (0.2)	2	2.2
NON-H	2.5 (0.2)	3	1.0
Binding energy contributions		4	2.4
$\Delta G_b$	–63.4 (4.0)	5	2.3
$\Delta U_{VDW}$	–56.2 (2.0)	6	2.2
$\Delta U_{elec}$	–3.9 (2.4)	7	1.3
$\Delta \Delta G_{s, np}$	–15.1 (0.8)	8	1.0
$\Delta \Delta G_{s, elec}$	11.8 (1.7)	9	2.0
		10	1.3
		Average	1.9 (0.6)

RMSD values are in Å; binding energy values are in kcal/mol.

than those in the simulations of MLN64 itself (cf. Table 1). Specifically, the ensemble-averaged backbone RMSD values for the secondary structure elements are 1.1 and 2.1 Å for the  $\beta$ -strand and helical regions, respectively, and 2.0 Å for the overall structure. As for the MLN64 simulations, these values reflect structural changes around the entrance of the cavity, although in this case changes were also located in other helical and loop regions (see sup-

plementary Fig. IV). Nevertheless, the overall architecture of the domain and the binding cavity is preserved.

The ring scaffold of the cholesterol deviates by 1.9 Å on average compared with the starting pose (Table 4). Although no flipping was observed in any of the simulations (see per-run RMSD values and time series in supplementary Fig. V), the ligand appears to be less stable than in the MLN64 simulations of the same binding mode, with a larger variability among independent runs (cf. Table 2 and supplementary Fig. III). Overall, the total binding energy calculated for cholesterol in the model of StAR-StART (Table 4) is  $\sim 10\%$  less favorable with respect to MLN64 (cf. Table 3). In particular, the most significant difference is observed in the electrostatic component of the protein-ligand interaction energy, which is more than 2-fold less favorable.

*Analysis of the binding mode of cholesterol in StAR versus MLN64.* The substitution of Ser362 in MLN64 by a Leu residue in the equivalent position of StAR (Leu199) is the underlying cause of the loss of favorable electrostatic interactions. Thus, although the ligand is somewhat locked in place in MLN64 by virtue of a hydrogen bond with Ser362, only short-lived hydrogen bonds with the backbone of Leu199 (13%) and with the side chain of Arg188 ( $\sim 5\%$ ) are observed in the ensemble of conformations obtained for StAR (Fig. 5). Representative configurations corresponding to these alternative hydrogen bonds in the StAR-StART complex are shown in Fig. 6. In addition, the

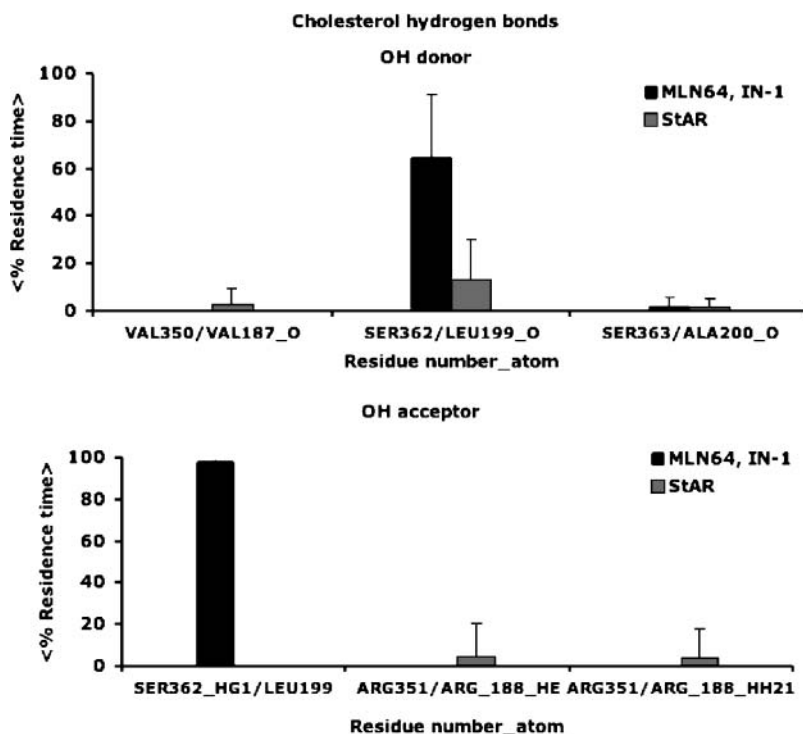
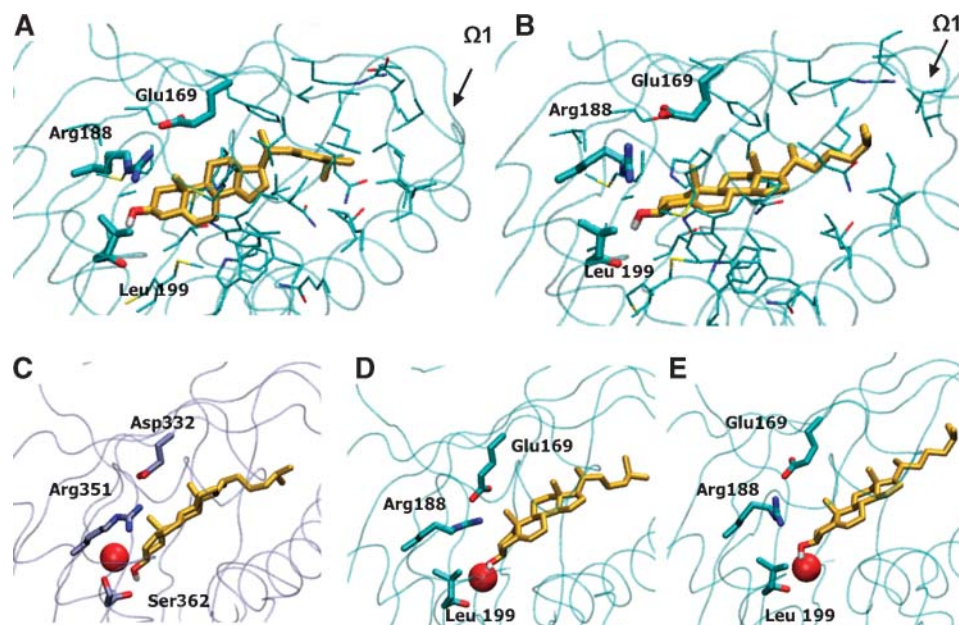


Fig. 5. Lifetime of the hydrogen bonds between the hydroxyl group of cholesterol (donor and acceptor) and residues in steroidogenic acute regulatory protein StAR-StART (gray) or MLN64-StAR/IN-1 (black), expressed as average percentages of the simulation times. For a given simulation, the residence time of a hydrogen bond is simply the fraction of the ensemble in which the bond is present. The error bars represent the SD over the simulation in each set.





**Fig. 6.** Close-up view of the binding conformation of cholesterol within StAR-StART. Two representative configurations of the simulated ensemble showing direct hydrogen bond interactions of the hydroxyl group of the cholesterol with the backbone of the residue of Leu199 (A) or the side chain of Arg188 (B) are depicted. Examples of the water-mediated interaction of cholesterol and the protein, as predicted by GRID, are shown for MLN64-StART (C) as well as StAR-StART (D, E).

ring and the flexible aliphatic chain strongly contribute to its interaction energy through a series of relatively unspecific hydrophobic interactions with residues facing into the cavity. Although equivalent contacts are found in MLN64 and StAR-StART complexes (see supplementary Fig. VI; cutoff of 3 Å), distinct contacts also exist as a result of slight differences in the orientation of the cholesterol ring (Fig. 6 vs. Fig. 3).

The absence of long-lasting specific hydrogen bonding contacts in StAR-StART suggests that water molecules may be mediating the interaction between ligand and protein in this case. By contrast, a direct interaction with Ser362 appears to be predominant in MLN64-StART. Given that this residue is conserved in all other putative or known cholesterol binders in the StART domain family (StarD4, StarD5, and StarD6) (28, 67), this difference might reflect specific functional needs in the case of StAR. Although only a few structures of protein-cholesterol complexes have been solved to date, these already include examples of both direct and water-mediated contacts for comparable binding site architectures and presumably similar mechanisms of uptake and release of the ligand. For instance, a specific hydrogen bond with the side chain of a tyrosine residue was observed in the crystal structure of the complex with  $\beta$ -cryptogin (1lri) (68), whereas a well-ordered network of water-mediated interactions was found in the hormone receptor ROR $\alpha$  (1n83) (44); two water bridges and a direct hydrogen bond with a glutamine side chain are also present in the recently reported complex of cholesterol with the oxysterol binding protein Osh4 (1zhy) (69).

To further explore the possible role of water-mediated hydrogen bonding, we analyzed the most probable occu-

pancy of water molecules within the cavity of both StART domains in the presence of cholesterol in an ensemble of 500 configurations extracted from our simulations using the GRID molecular modeling software (70) ([www.moldiscovery.com](http://www.moldiscovery.com); see Refs. 71–73 for successful predictions using this application). Among the configurations of the MLN64-StAR complex, in which a direct interaction with Ser362 is almost always present (99%), only in 71 cases (14%) did GRID predict one or more water molecules that could potentially form a hydrogen bond (based on a distance criterion) with the hydroxyl group of cholesterol and either the side chain of Ser362 (37 cases) or those of both Ser362 and Arg351 (34 cases) (Fig. 6C). By contrast, in the ensemble of configurations of StAR-StART, a significantly higher number of cases were found in which water molecules could form concurrent hydrogen bonds with cholesterol and the receptor is predicted: 183 of 500 configurations (37%). Specifically, one or more water molecules in close proximity from either the carbonyl group of Leu199 and/or the guanidinium group of Arg188 are found in 38% of the configurations in which there is a lack of specific interaction of the cholesterol with the residues in the protein (73% of the ensemble) (Fig. 6D). Of those configurations of StAR-StART in which cholesterol forms a hydrogen bond to Arg188 (9% of the ensemble), at least one water molecule is predicted in 91% of the cases (Fig. 6E). In the configurations in which there is a direct interaction of cholesterol with residues located at the end of the cavity (18% of the ensemble, mainly with Leu199), a water molecule is found in only 3% of the cases. In the great majority of the 183 cases mentioned above, the water-mediated hydrogen bond network between cho-

lesterol and the receptor is predicted to involve a single water molecule, which would interact predominantly with the carbonyl group of Leu199 only (133 cases) but also with the side chain of Arg188 (50 cases). Interestingly, mutations of the side chains of Arg188 and glutamate 169 (Glu169), which form an ion pair, have indeed been shown to lead to a loss of function (13, 74), although it is not clear whether this reflects an actual involvement in ligand binding (20, 74) or simply a structural role during folding of the polypeptide chain (13, 34, 75).

In summary, this analysis is consistent with the notion that the direct hydrogen bond of cholesterol to Ser362, present in MLN64-StART, could be replaced by a water-mediated interaction with residues located at the end of the cavity in StAR-StART. The water-mediated interaction might also include the side chain of Arg188 (Arg351 in MLN64), which is conserved or substituted by a polar residue in other cholesterol binders of the StART family. Additional simulations including solvent explicitly will help to further explore the microscopic properties of these water-mediated interactions.

From an experimental viewpoint, it would be of great interest to determine how the exchange of the Ser and Leu residues at the end of the cavity affects the binding properties of MLN64 and StART. Nonbulky esters, ethers, or other related compounds at the cholesterol head could be used to investigate the possibility of a water-mediated interaction network in the binding cavity. A similar idea has been applied to the study of cholesterol binding to the hormone receptor ROR $\alpha$ , which was initially found to involve several water bridges between ligand and protein (1n83). The subsequent crystal structure of the complex with cholesterol sulfate (1s0x) revealed that most of the water-mediated contacts can be replaced by direct protein-sulfate interactions, whereas the ligand was seen to be only slightly shifted toward the polar end of the binding pocket (76).

#### Simulations of cholesterol release from the cavity of StAR and MLN64 StART domains

The mechanism of transfer of cholesterol between membranes and the interior of StART domains remains to be elucidated. At present, only the role of the C-terminal helix and adjacent loops in mediating the interaction of these domains with the membrane has been established somewhat conclusively, specifically through proteolysis and sequence-truncation experiments (58, 77, 78). The charge distribution of StAR-StART is consistent with this orientation for the membrane association. It is also clear that upon interaction with the membrane, StART domains must undergo a conformational change to facilitate the uptake or release of their ligands. Nonetheless, the extent of this change and the structural elements involved remain a matter of debate (20, 31, 58, 79).

Based primarily on biophysical studies, it has been proposed that the transfer of cholesterol in StAR and MLN64 may involve a transition to a molten-globule state, which would entail noticeable changes in the secondary and possibly tertiary structure of the protein as a result of the interaction with the acidic mitochondrial outer mem-

brane (80). Specifically, the disruption of electrostatic interactions stabilizing the arrangement of the C-terminal helix, such as the Asp106-Arg272 ion pair in StAR, would lead to changes in the protein fold and the exposure of the binding site to the lipid phase (58, 79). This notion originates from the fact that circular dichroism and fluorescence spectra change under low pH conditions, either in solution (29, 78, 80, 81) or in the presence of zwitterionic synthetic membranes (82, 83), and from the observation that engineered disulfide bridges that prevent the transition to the molten globule in StAR (S100C/S261C and D106C/A268C; see Fig. 8 below) also lead to the loss of cholesterol binding capacity and steroidogenic activity (79).

By contrast, crystallographic data and the structural and functional similarity of StART domains with other lipid binding proteins suggest that the uptake and release of cholesterol may simply involve the transient opening of its narrow entrance without a significant perturbation of the overall fold of the domain (20, 31, 84). This mechanism, often referred to as "clam-shell," is supported by the comparison of the *apo* structure of MLN64-StART and the StART domain of PCTP in complex with a PC lipid, which reveals that the most significant differences occur in the positioning of loop  $\Omega$ 1 and the C-terminal helix (31). Analogous structural changes involving the so-called lipid-exchange loop are also apparent when comparing alternative conformations of the PITP $\alpha$  binding protein, which is structurally similar to StART (62, 63, 85). On the other hand, recent biophysical studies have indirectly suggested that the interaction of PITP with membrane surfaces may lead to more significant changes in the protein conformation (60).

To gain additional insights into the potential conformational changes required for the uptake and release of cholesterol, and to qualitatively characterize the corresponding pathway, we carried out multiple MD simulations in which cholesterol is steered out of the cavity of StAR-StART and MLN64-StART (see Methods for further details). In spite of the differences in the starting configuration of the complex, force constants, and steering rates, the same overall conclusions can be drawn from several independent simulations. First, analyses of the time series of the RMSD of the cholesterol ring (Fig. 7A), per-residue contributions to that of the backbone (Fig. 7C), and the relative displacements of loops adjacent to the C-terminal  $\alpha$ -helix (Fig. 7B) suggest that cholesterol release only requires the opening of loop  $\Omega$ 1 (residues 172–181 of StAR and residues 335–344 of MLN64). For example, the backbone RMSD of Gly176 of StAR, located in that loop, increases to 10–14 Å relative to the starting conformation. Accordingly, a correlated increase in the distances between Gly176 and residues in the C-terminal helix is also observed (Fig. 7B). By contrast, the RMSD of all of the residues other than the loop remains in the 2–3 Å range (Fig. 7C).

In Fig. 8 representative configurations taken from the steered MD simulations of cholesterol release from MLN64 and StAR-StART are depicted alongside the closed and putatively open states of PITP $\alpha$ . As discussed above,

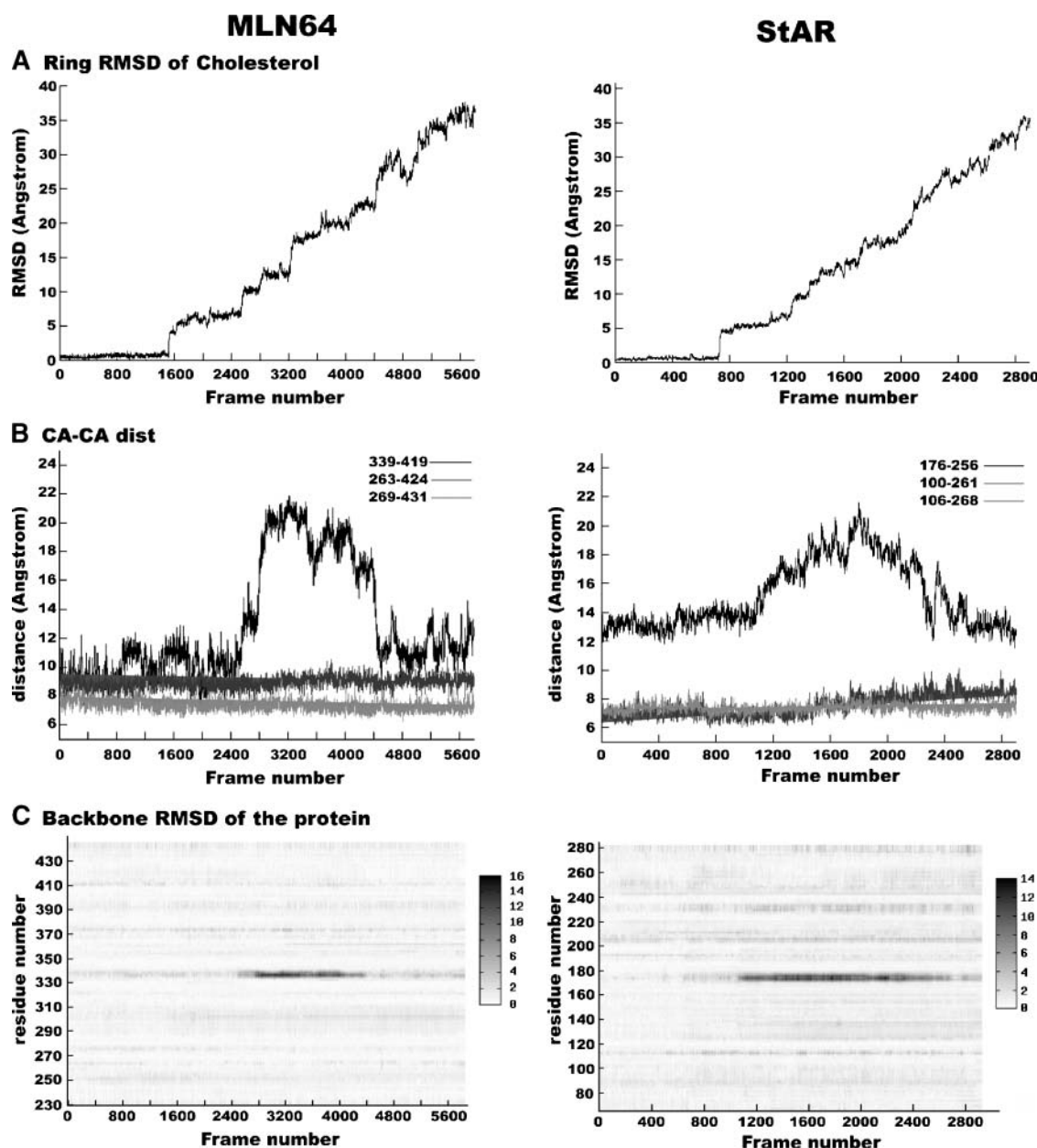


**Fig. 7.** Steered MD simulations of cholesterol release from the MLN64-StART and StAR-StART cavity (force constant of  $2 k_B T \text{\AA}^{-2}$  and rates of  $0.01 \text{\AA ps}^{-1}$  and  $0.02 \text{\AA ps}^{-2}$ , respectively). **A:** Cholesterol displacements during the steered simulation in terms of the RMSD of the ring moiety with respect to the starting position as a function of the frame number (2 per ps). **B:** Time series showing the C $\alpha$ -C $\alpha$  distances between residue pairs in the C-terminal  $\alpha$ -helix and loops  $\beta$ 1- $\beta$ 2 (MLN64, Lys263-Ala424 and Asp269-Ala431; StAR, Ser100-Ser261 and Asp106-Ala268) and  $\Omega$ 1 ( $\beta$ 5- $\beta$ 6) (MLN64, Gly339-Ile419; StAR, Gly176-Ile256) during the steered simulation. **C:** Per-residue backbone RMSD of the protein during these simulations of cholesterol release showing the transient opening of loop  $\Omega$ 1.

these simulations indicate that the structural changes involved in cholesterol release entail primarily the  $\Omega$ 1 loop, which was observed to adopt an open conformation as cholesterol leaves the binding cavity and to subsequently close once the ligand is in the bulk. Although the process of release was simulated far from equilibrium, comparison of PITP $\alpha$  in its closed and open conformations indicates that the overall conclusions from this analysis are very plausible.

Analysis of the hydrogen bonds between ligand and protein during the steered simulations reveals a putative

pathway comprising a series of transient states stabilized by specific interactions (**Fig. 9**). In the case of StAR, hydrogen bonds of the cholesterol hydroxyl group are formed with the side chains of residues within the cavity, such as threonine 223 (Thr223), Arg188, Glu169, and histidine 220 (His220) (all of which line the  $\beta$ -stranded walls of the cavity that are opposed to the C-terminal  $\alpha$ -helix). Interactions with the side chains of Asn148 and Asn150 (located in the region between  $\beta$ 3 and  $\beta$ 4 and contributing to the roof of the binding site) and Thr263 (at the N terminus of the C-terminal helix) (**Fig. 9**) are also



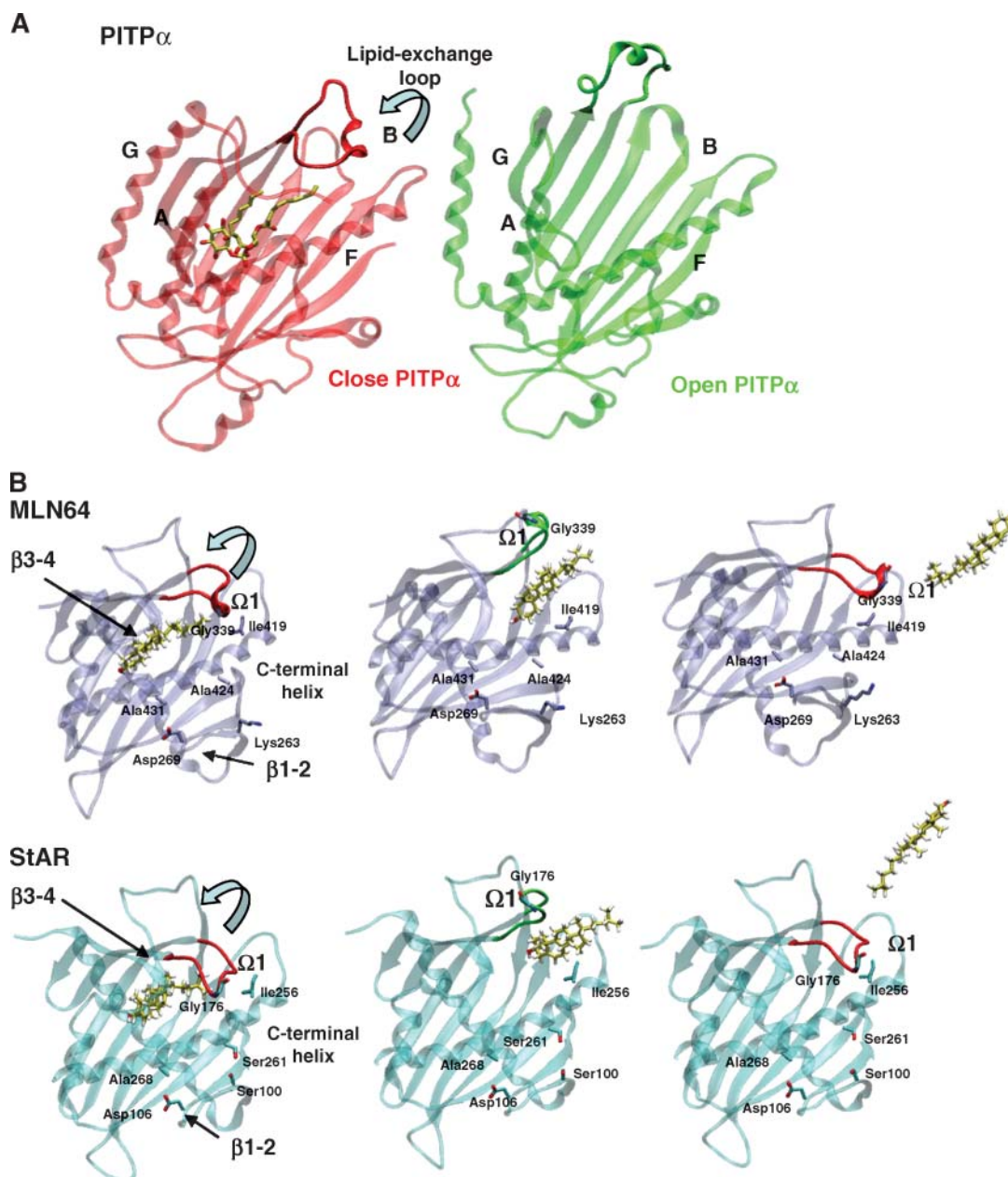


**Fig. 8.** A: Three-dimensional structure of the closed (red) and open (green) configurations of phosphatidylinositol transfer protein  $\alpha$  (PITP $\alpha$ ). The opening of the lipid-exchange loop putatively associated with ligand uptake and release is highlighted (the structure derived from a homodimeric complex where this loop is domain-swapped) (62). B: Initial, intermediate, and final conformations of MLN64-StART (top) and StAR-StART (bottom) from the steered MD simulation of cholesterol release (force constant of  $2 \text{ k}_B T \text{ \AA}^{-2}$  and rates of  $0.01 \text{ \AA ps}^{-1}$  and  $0.02 \text{ \AA ps}^{-2}$ , respectively). Loop  $\Omega$ 1 is highlighted in its closed (red) and open (green) conformations. See also movies in the supplementary material.

observed. Overall, these intermediate states can be correlated with the stepwise displacements of the cholesterol as it is steered out of the cavity and the concomitant opening of loop  $\Omega$ 1 (Figs. 7, 8). Loss of the interaction with Asn150 appears to be the last step before the complete release of cholesterol. Interestingly, three of these residues have been demonstrated to be important for the activity of StAR, namely Glu169 [mutated to Thr and lysine (Lys)/Gly in the lipid adrenal hyperplasia] (13), Arg188 [mutated in vitro to methionine (Met) together with a mutation to

Leu of Glu169, with which it forms a salt bridge] (74), and Asn148 (previously related to the specificity of StAR and MLN64 for cholesterol together with Met144) (20, 23, 31). Their potential role in the stabilization of intermediate states during cholesterol uptake and release provides a plausible rationale for their functional importance; therefore, we propose that further mutagenesis studies targeting these residues (i.e., Thr223, His220, Asn150, and Thr263) may provide new insights into the mechanism of sterol binding.

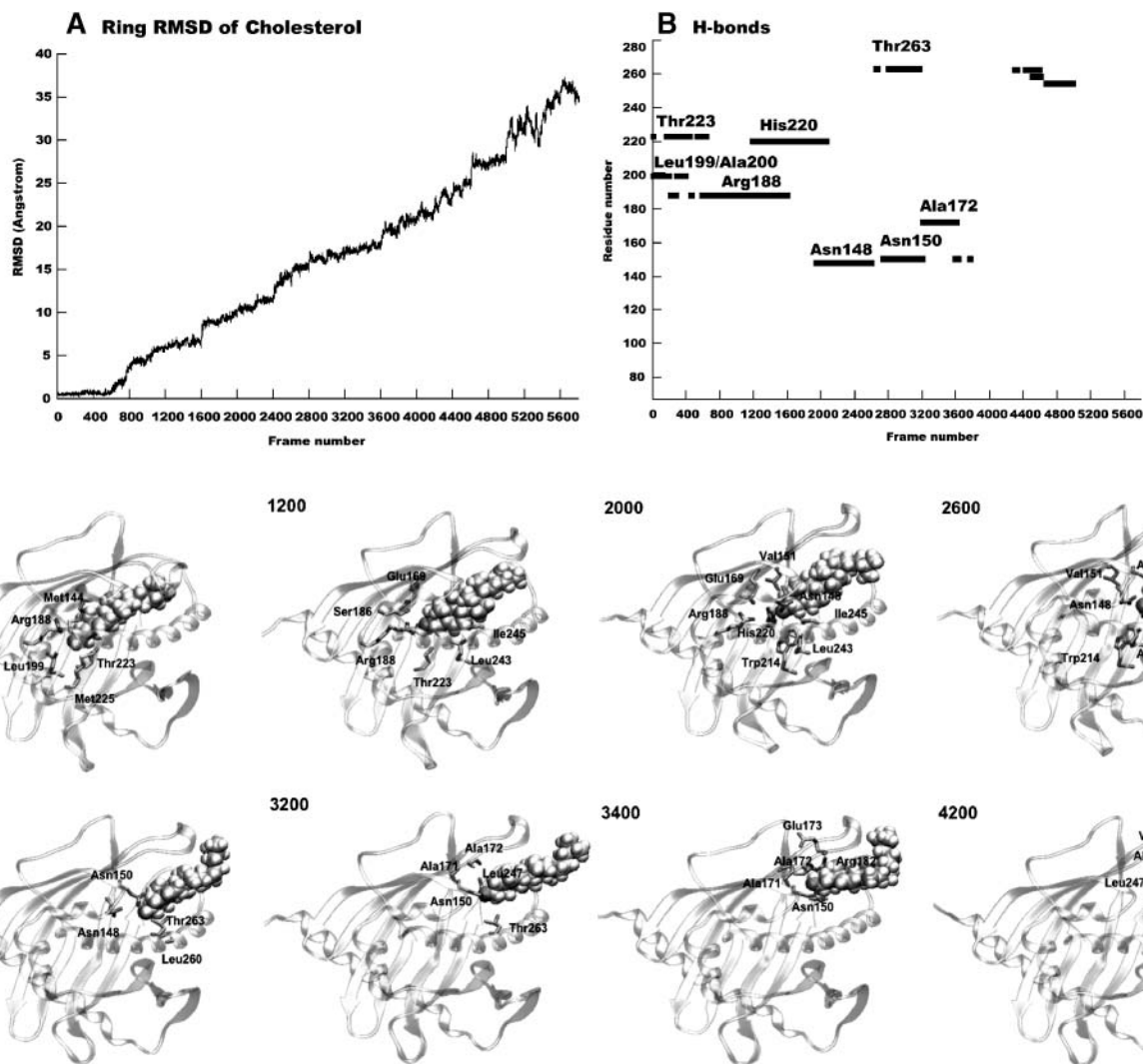


**Fig. 9.** Steered MD simulation of cholesterol release from the StAR-StART cavity (force constant of  $8 \text{ k}_B T \text{ \AA}^{-2}$  and rate of  $0.01 \text{ \AA ps}^{-1}$ ). **A:** Cholesterol displacements during the steered simulation in terms of the RMSD of the ring moiety with respect to the starting position as a function of the frame number (2 per ps). **B:** Time series analysis of the hydrogen bonds formed between the cholesterol hydroxyl group and the side chains of residues within the cavity during the steered simulation. **C:** Representative configurations of the complex of StAR-StART and cholesterol from the simulated ensemble. The sequential interactions of cholesterol with residues lining the binding cavity of StAR-StART are indicated.

Similar conclusions can be drawn from analogous steered MD simulations of MLN64-StART (data not shown). In both cases, a lid-like transient opening of loop  $\Omega 1$  seems to provide a sufficient conformational change that would allow cholesterol egress from the StART binding site, without further substantial rearrangement of the structure (Figs. 7, 8; see movies in supplementary material). In conflict with the molten-globule hypothesis, these simulations reveal no significant changes in the distances between those residues involved in the stabilization of the C-terminal helix or between the residues engineered to form disulfide bridges that were recently reported to abolish cholesterol binding (79) (Fig. 8; see supplementary Fig. VII). Thus, we hypothesize that the latter experimental observation might simply reflect a reduction in the binding affinity of the domain caused by subtle but critical structural changes, rather than a perturbation of the mechanism of opening of

the binding cavity. Supporting this notion, conformational changes upon disulfide bridge formation have been reported (86) and characterized at atomic resolution for the reduced and oxidized forms of proteins such as SOD1 (87) and the members of the peroxiredoxin family (88), as well as in the case of engineered disulfide mutants. For example, the C21-C142 mutant of T4 lysozyme, whose reduced-form structure is almost identical to that of the wild-type protein, alters its conformation upon oxidation, causing the  $\alpha$  carbons of the cysteine (Cys) pair to move toward each other by  $2.5 \text{ \AA}$  (89). A careful analysis based on the simulations of the protein-cholesterol complexes reported above suggests that the engineered disulfide bridges reported by Baker, Yaworsky, and Miller (79) could have an impact on equilibrium ligand binding. Direct substitutions of Cys residues in the ensemble of 10,000 configurations of StAR-StART yield average S-S distances of  $5.7 \pm 1.4$  and  $3.3 \pm 0.9 \text{ \AA}$  for

the Ser100/Ser261 and Asp106/Ala268 pairs, respectively. Similar substitutions in the ensemble of MLN64-StART (IN-1) yield average distances of  $5.9 \pm 0.3$  and  $2.6 \pm 0.3$  Å for the Lys263/Ala424 and Asp269/Ala431 pairs, respectively (those distances are 4.1 and 2.8 Å in the crystal structure of the *apo* MLN64-StART). Because the S-S distance in disulfide bridges is  $\sim 2.0$  Å, it seems likely that the formation of a disulfide bond will give rise to local structural stress that could affect ligand binding. Unfortunately, the current computational framework precludes us from fully elucidating the nature of such subtle changes and their potential impact on the binding process.

The binding properties of StART domains are known to be highly sensitive to subtle changes in the C-terminal region. For example, one of the three available atomic structures of PCTP-StART in complex with PC lipids reveals a disulfide bond between Cys63 and Cys207 (in the loop joining  $\beta 3$ - $\alpha 2$  and the C-terminal helix, respectively). Although the formation of this bond induces only slight local changes in structure and is believed not to affect the function of the protein, the specific activities of the C63A and C63S mutants were reduced by 22% and 55%, respectively, with respect to the wild-type protein (31). In StAR itself, missense mutations of residues located in the C-terminal helix and adjacent loops lead to complete malfunction, as in the pathological mutants L260P (9),  $\Delta$ R272, and L275P (90), or to partial loss of activity, as in the F267Y, D246A, and K248M *in vitro* mutants. By contrast, more conservative mutations at the C terminus of the helix, such as H270Y, S277A, and C285S, have no significant impact on the activity (90).


In summary, the present analysis is consistent with the view that the uptake and release of cholesterol could take place via conformational changes localized at the entrance of the binding cavity while preserving the secondary structure and overall fold of the protein. We thus speculate that the role of loop  $\Omega 1$  in StAR domains may be analogous to that of the lipid-exchange loop in PITP $\alpha$  (62, 85) (Fig. 8A). Mutagenesis studies focused on this region of the protein, such as those by Baker, Yaworsky, and Miller (79) (e.g., substituting the Ala175-Val259 pair), or the introduction of spectroscopic probes and a range of biophysical methods, could help assess the validity of this hypothesis. The conception of a multistep pathway in and out of the binding cavity via a localized conformational change in the structure could be implicated in the function of other sterol/lipid-carrier proteins, such as PITP $\alpha$  (91), PITP $\beta$  (92), Niemann-Pick type C2 protein (93), sterol carrier protein-2 (94), plant nonspecific lipid transfer proteins (95–97), elicitors such as  $\beta$ -cryptogein (68, 98–100), the ligand binding domain of ROR $\alpha$  (44, 76), sterol esterase (101), cholesterol oxidase (102), oxysterol binding protein-related proteins (69), and even fatty acid binding proteins (103).

## CONCLUSIONS

Computational methods have been used to model the three-dimensional atomic structure of the complex of cho-

lesterol with the homologous StART domains of the human proteins MLN64 and StAR and to investigate the cholesterol uptake and release mechanism.

Overall, no major changes in the protein structure were observed upon inclusion of cholesterol, supporting the view that these domains contain a preformed cavity that is suitable in shape and size for cholesterol binding. Both three-dimensional models present similar binding features, although the substitution of residue Ser362 in MLN64 by Leu199 in StAR appears to weaken the strength of cholesterol binding. The major contribution to the ligand-protein interactions is attributable to nonpolar contacts with side chains lining the binding cavity, although electrostatic interactions could play an important role in the fine-tuning of the binding mode. Our analysis suggests that a hydrogen bond could exist between the hydroxyl group of cholesterol and MLN64-Ser362 and that this interaction is replaced by a water bridge with the backbone of Leu199 in StAR. In addition, we propose that Arg351/Arg188 might also be involved in a water-mediated interaction network similar to those observed in other cholesterol binding proteins.

Using steered MD simulations, a lid-like transient opening restricted to loop  $\Omega 1$  is sufficient to allow the cholesterol egress from the StAR-StART binding site, without any significant rearrangement of the protein structure. Furthermore, a series of hydrogen bond contacts between cholesterol and the side chains of residues lining the cavity appear to stabilize several intermediate states while the ligand is released. This observation suggests an explanation for the known functional importance of some of these residues, which otherwise appear not to participate directly in the stabilization of cholesterol. 

The authors thank Zoe Cournia and Jeremy Smith for sending us their parameter set for cholesterol, Ángel R. Ortiz for sharing the program Flexdock, and Manuel Pastor for insightful discussion on the GRID application. M.M. gratefully acknowledges a postdoctoral fellowship from the Ramón Areces Foundation, Spain. This work was supported by National Institutes of Health Grant DK-27083 to F.R.M.

## REFERENCES

1. Stocco, D. M. 1999. Steroidogenic acute regulatory (StAR) protein: what's new? *Bioessays*. **21**: 768–775.
2. Sierra, A. 2004. Neurosteroids: the StAR protein in the brain. *J. Neuroendocrinol.* **16**: 787–793.
3. Soccio, R. E., and J. L. Breslow. 2003. StAR-related lipid transfer (START) proteins: mediators of intracellular lipid metabolism. *J. Biol. Chem.* **278**: 22183–22186.
4. Stocco, D. M., and B. J. Clark. 1996. Role of the steroidogenic acute regulatory protein (StAR) in steroidogenesis. *Biochem. Pharmacol.* **51**: 197–205.
5. Christenson, L. K., and J. F. Strauss, 3rd. 2000. Steroidogenic acute regulatory protein (StAR) and the intramitochondrial translocation of cholesterol. *Biochim. Biophys. Acta.* **1529**: 175–187.
6. Strauss, J. F., 3rd, C. B. Kallen, L. K. Christenson, H. Watari, L. Devoto, F. Arakane, M. Kiriakidou, and T. Sugawara. 1999. The steroidogenic acute regulatory protein (StAR): a window into the complexities of intracellular cholesterol trafficking. *Recent Prog. Horm. Res.* **54**: 369–394 (discussion 394–395).



7. Petrescu, A. D., A. M. Gallegos, Y. Okamura, J. F. Strauss, 3rd, and F. Schroeder. 2001. Steroidogenic acute regulatory protein binds cholesterol and modulates mitochondrial membrane sterol domain dynamics. *J. Biol. Chem.* **276**: 36970–36982.
8. Manna, P. R., and D. M. Stocco. 2005. Regulation of the steroidogenic acute regulatory protein expression: functional and physiological consequences. *Curr. Drug Targets Immune Endocr. Metabol. Disord.* **5**: 93–108.
9. Fluck, C. E., A. Maret, D. Mallet, S. Portrat-Doyen, J. C. Acher-mann, B. Leheup, G. E. Theintz, P. E. Mullis, and Y. Morel. 2005. A novel mutation L260P of the steroidogenic acute regulatory protein gene in three unrelated patients of Swiss ancestry with congenital lipid adrenal hyperplasia. *J. Clin. Endocrinol. Metab.* **90**: 5304–5308.
10. Gonzalez, A. A., M. L. Reyes, C. A. Carvajal, J. A. Tobar, L. M. Mosso, P. Baquedano, A. Solar, A. Venegas, and C. E. Fardella. 2004. Congenital lipid adrenal hyperplasia caused by a novel splicing mutation in the gene for the steroidogenic acute regulatory protein. *J. Clin. Endocrinol. Metab.* **89**: 946–951.
11. Fujieda, K., K. Okuhara, S. Abe, T. Tajima, T. Mukai, and J. Nakae. 2003. Molecular pathogenesis of lipid adrenal hyperplasia and adrenal hypoplasia congenita. *J. Steroid Biochem. Mol. Biol.* **85**: 483–489.
12. Stocco, D. M. 2002. Clinical disorders associated with abnormal cholesterol transport: mutations in the steroidogenic acute regulatory protein. *Mol. Cell. Endocrinol.* **191**: 19–25.
13. Bose, H. S., T. Sugawara, J. F. Strauss, 3rd, and W. L. Miller. 1996. The pathophysiology and genetics of congenital lipid adrenal hyperplasia. International Congenital Lipoid Adrenal Hyperplasia Consortium. *N. Engl. J. Med.* **335**: 1870–1878.
14. Lin, D., T. Sugawara, J. F. Strauss, 3rd, B. J. Clark, D. M. Stocco, P. Saenger, A. Rogol, and W. L. Miller. 1995. Role of steroidogenic acute regulatory protein in adrenal and gonadal steroidogenesis. *Science*. **267**: 1828–1831.
15. Christenson, L. K., and J. F. Strauss, 3rd. 2001. Steroidogenic acute regulatory protein: an update on its regulation and mechanism of action. *Arch. Med. Res.* **32**: 576–586.
16. Arakane, F., C. B. Kallen, H. Watari, J. A. Foster, N. B. Sepuri, D. Pain, S. E. Stayrook, M. Lewis, G. L. Gerton, and J. F. Strauss, 3rd. 1998. The mechanism of action of steroidogenic acute regulatory protein (StAR). StAR acts on the outside of mitochondria to stimulate steroidogenesis. *J. Biol. Chem.* **273**: 16339–16345.
17. Arakane, F., T. Sugawara, H. Nishino, Z. Liu, J. A. Holt, D. Pain, D. M. Stocco, W. L. Miller, and J. F. Strauss, 3rd. 1996. Steroidogenic acute regulatory protein (StAR) retains activity in the absence of its mitochondrial import sequence: implications for the mechanism of StAR action. *Proc. Natl. Acad. Sci. USA*. **93**: 13731–13736.
18. Wang, X., Z. Liu, S. Eimerl, R. Timberg, A. M. Weiss, J. Orly, and D. M. Stocco. 1998. Effect of truncated forms of the steroidogenic acute regulatory protein on intramitochondrial cholesterol transfer. *Endocrinology*. **139**: 3903–3912.
19. Ponting, C. P., and L. Aravind. 1999. START: a lipid-binding domain in StAR, HD-ZIP and signalling proteins. *Trends Biochem. Sci.* **24**: 130–132.
20. Tsujishita, Y., and J. H. Hurley. 2000. Structure and lipid transport mechanism of a StAR-related domain. *Nat. Struct. Biol.* **7**: 408–414.
21. Maxfield, F. R., and I. Tabas. 2005. Role of cholesterol and lipid organization in disease. *Nature*. **438**: 612–621.
22. Schrick, K., D. Nguyen, W. M. Karłowski, and K. F. Mayer. 2004. START lipid/sterol-binding domains are amplified in plants and are predominantly associated with homeodomain transcription factors. *Genome Biol.* **5**: R41.1–R41.16.
23. Alpy, F., and C. Tomasetto. 2005. Give lipids a START: the StAR-related lipid transfer (START) domain in mammals. *J. Cell Sci.* **118**: 2791–2801.
24. Soccio, R. E., and J. L. Breslow. 2004. Intracellular cholesterol transport. *Arterioscler. Thromb. Vasc. Biol.* **24**: 1150–1160.
25. Iyer, L. M., E. V. Koonin, and L. Aravind. 2001. Adaptations of the helix-grip fold for ligand binding and catalysis in the START domain superfamily. *Proteins*. **43**: 134–144.
26. Alpy, F., V. K. Latchumanan, V. Keding, A. Janoshazi, C. Thiele, C. Wendling, M. C. Rio, and C. Tomasetto. 2005. Functional characterization of the MENTAL domain. *J. Biol. Chem.* **280**: 17945–17952.
27. Alpy, F., and C. Tomasetto. 2006. MLN64 and MENTHO, two mediators of endosomal cholesterol transport. *Biochem. Soc. Trans.* **34**: 343–345.
28. Strauss, J. F., 3rd, T. Kishida, L. K. Christenson, T. Fujimoto, and H. Hiroi. 2003. START domain proteins and the intracellular trafficking of cholesterol in steroidogenic cells. *Mol. Cell. Endocrinol.* **202**: 59–65.
29. Tuckey, R. C., H. S. Bose, I. Czerwionka, and W. L. Miller. 2004. Molten globule structure and steroidogenic activity of N-218 MLN64 in human placental mitochondria. *Endocrinology*. **145**: 1700–1707.
30. Romanowski, M. J., R. E. Soccio, J. L. Breslow, and S. K. Burley. 2002. Crystal structure of the *Mus musculus* cholesterol-regulated START protein 4 (StarD4) containing a StAR-related lipid transfer domain. *Proc. Natl. Acad. Sci. USA*. **99**: 6949–6954.
31. Roderick, S. L., W. W. Chan, D. S. Agate, L. R. Olsen, M. W. Vetting, K. R. Rajashankar, and D. E. Cohen. 2002. Structure of human phosphatidylcholine transfer protein in complex with its ligand. *Nat. Struct. Biol.* **9**: 507–511.
32. Shen, Y., S. Goldsmith-Fischman, H. S. Atreya, T. Acton, L. Ma, R. Xiao, B. Honig, G. T. Montelione, and T. Szyperki. 2005. NMR structure of the 18 kDa protein CC1736 from *Caulobacter crescentus* identifies a member of the START domain superfamily and suggests residues mediating substrate specificity. *Proteins*. **58**: 747–750.
33. Nakabayashi, M., N. Shibata, H. Komori, Y. Ueda, H. Iino, A. Ebihara, S. Kuramitsu, and Y. Higuchi. 2005. Structure of a conserved hypothetical protein, TTHA0849 from *Thermus thermophilus* HB8, at 2.4 Å resolution: a putative member of the StAR-related lipid-transfer (START) domain superfamily. *Acta Crystallograph. Sect. F Struct. Biol. Cryst. Commun.* **61**: 1027–1031.
34. Bose, H. S., M. A. Baldwin, and W. L. Miller. 1998. Incorrect folding of steroidogenic acute regulatory protein (StAR) in congenital lipid adrenal hyperplasia. *Biochemistry*. **37**: 9768–9775.
35. Brooks, B. R., R. E. Bruccoleri, B. D. Olafson, D. J. States, S. Swaminathan, and M. Karplus. 1983. CHARMM: a program for macromolecular energy, minimization, and dynamics calculations. *J. Comput. Chem.* **4**: 187–217.
36. MacKerell, A. D., Jr., M. Feig, and C. L. Brooks, 3rd. 2004. Improved treatment of the protein backbone in empirical force fields. *J. Am. Chem. Soc.* **126**: 698–699.
37. Pitman, M. C., F. Suits, A. D. Mackerell, Jr., and S. E. Feller. 2004. Molecular-level organization of saturated and polyunsaturated fatty acids in a phosphatidylcholine bilayer containing cholesterol. *Biochemistry*. **43**: 15318–15328.
38. Im, W., M. S. Lee, and C. L. Brooks, 3rd. 2003. Generalized Born model with a simple smoothing function. *J. Comput. Chem.* **24**: 1691–1702.
39. Nina, M., W. Im, and B. Roux. 1999. Optimized atomic radii for protein continuum electrostatics solvation forces. *Biophys. Chem.* **78**: 89–96.
40. Ciccotti, G., and J. Berendsen. 1977. Numerical integration of the Cartesian equations of motion of a system with constraints: molecular dynamics of n-alkanes. *J. Comput. Phys.* **23**: 327–341.
41. Deshpande, N., K. J. Address, W. F. Bluhm, J. C. Merino-Ott, W. Townsend-Merino, Q. Zhang, C. Knezevich, L. Xie, L. Chen, Z. Feng, et al. 2005. The RCSB Protein Data Bank: a redesigned query system and relational database based on the mmCIF schema. *Nucleic Acids Res.* **33**: D233–D237.
42. Berman, H. M., T. N. Bhat, P. E. Bourne, Z. Feng, G. Gilliland, H. Weissig, and J. Westbrook. 2000. The Protein Data Bank and the challenge of structural genomics. *Nat. Struct. Biol.* **7** (Suppl.): 957–959.
43. Bernstein, F. C., T. F. Koetzle, G. J. Williams, E. F. Meyer, Jr., M. D. Brice, J. R. Rodgers, O. Kennard, T. Shimanouchi, and M. Tasumi. 1977. The Protein Data Bank: a computer-based archival file for macromolecular structures. *J. Mol. Biol.* **112**: 535–542.
44. Kallen, J. A., J. M. Schlaeppli, F. Bitsch, S. Geisse, M. Geiser, I. Delhon, and B. Fournier. 2002. X-ray structure of the hRORalpha LBD at 1.63 Å: structural and functional data that cholesterol or a cholesterol derivative is the natural ligand of RORalpha. *Structure*. **10**: 1697–1707.
45. Murcia, M., and A. R. Ortiz. 2004. Virtual screening with flexible docking and COMBINE-based models. Application to a series of factor Xa inhibitors. *J. Med. Chem.* **47**: 805–820.
46. Hartigan, J. A. 1975. Clustering Algorithms. John Wiley & Sons, Inc., New York.
47. Roux, B., and T. Simonson. 1999. Implicit solvent models. *Biophys. Chem.* **78**: 1–20.
48. Thompson, J. D., D. G. Higgins, and T. J. Gibson. 1994. CLUSTAL W: improving the sensitivity of progressive multiple sequence align-

- ment through sequence weighting, position-specific gap penalties and weight matrix choice. *Nucleic Acids Res.* **22**: 4673–4680.
49. Canutescu, A. A., A. A. Shelenkov, and R. L. Dunbrack, Jr. 2003. A graph-theory algorithm for rapid protein side-chain prediction. *Protein Sci.* **12**: 2001–2014.
  50. Woo, H. J., and B. Roux. 2005. Calculation of absolute protein-ligand binding free energy from computer simulations. *Proc. Natl. Acad. Sci. USA*. **102**: 6825–6830.
  51. Chen, W., C. E. Chang, and M. K. Gilson. 2004. Calculation of cyclodextrin binding affinities: energy, entropy, and implications for drug design. *Biophys. J.* **87**: 3035–3049.
  52. Boresch, S., F. Tettinger, M. Leitgeb, and M. Karplus. 2003. Absolute binding free energies: a quantitative approach for their calculation. *J. Phys. Chem. B*. **107**: 9535–9551.
  53. Luo, H., and K. Sharp. 2002. On the calculation of absolute macromolecular binding free energies. *Proc. Natl. Acad. Sci. USA*. **99**: 10399–10404.
  54. Feig, M., and C. L. Brooks, 3rd. 2004. Recent advances in the development and application of implicit solvent models in biomolecule simulations. *Curr. Opin. Struct. Biol.* **14**: 217–224.
  55. Ferrara, P., H. Gohlke, D. J. Price, G. Klebe, and C. L. Brooks, 3rd. 2004. Assessing scoring functions for protein-ligand interactions. *J. Med. Chem.* **47**: 3032–3047.
  56. Bose, H. S., V. R. Lingappa, and W. L. Miller. 2002. The steroidogenic acute regulatory protein, StAR, works only at the outer mitochondrial membrane. *Endocr. Res.* **28**: 295–308.
  57. Bose, H., V. R. Lingappa, and W. L. Miller. 2002. Rapid regulation of steroidogenesis by mitochondrial protein import. *Nature*. **417**: 87–91.
  58. Yaworsky, D. C., B. Y. Baker, H. S. Bose, K. B. Best, L. B. Jensen, J. D. Bell, M. A. Baldwin, and W. L. Miller. 2005. pH-dependent interactions of the carboxyl-terminal helix of steroidogenic acute regulatory protein with synthetic membranes. *J. Biol. Chem.* **280**: 2045–2054.
  59. Phillips, S. E., P. Vincent, K. E. Rizzieri, G. Schaaf, V. A. Bankaitis, and E. A. Gaucher. 2006. The diverse biological functions of phosphatidylinositol transfer proteins in eukaryotes. *Crit. Rev. Biochem. Mol. Biol.* **41**: 21–49.
  60. Tremblay, J. M., J. R. Unruh, C. K. Johnson, and L. R. Yarbrough. 2005. Mechanism of interaction of PITPalpha with membranes: conformational changes in the C-terminus associated with membrane binding. *Arch. Biochem. Biophys.* **444**: 112–120.
  61. Tilley, S. J., A. Skippen, J. Murray-Rust, P. M. Swigart, A. Stewart, C. P. Morgan, S. Cockcroft, and N. Q. McDonald. 2004. Structure-function analysis of human [corrected] phosphatidylinositol transfer protein alpha bound to phosphatidylinositol. *Structure*. **12**: 317–326.
  62. Schouten, A., B. Agianian, J. Westerman, J. Kroon, K. W. Wirtz, and P. Gros. 2002. Structure of apo-phosphatidylinositol transfer protein alpha provides insight into membrane association. *EMBO J.* **21**: 2117–2121.
  63. Yoder, M. D., L. M. Thomas, J. M. Tremblay, R. L. Oliver, L. R. Yarbrough, and G. M. Helmkamp, Jr. 2001. Structure of a multifunctional protein. Mammalian phosphatidylinositol transfer protein complexed with phosphatidylcholine. *J. Biol. Chem.* **276**: 9246–9252.
  64. Ohvo-Rekila, H., B. Ramstedt, P. Leppimäki, and J. P. Slotte. 2002. Cholesterol interactions with phospholipids in membranes. *Prog. Lipid Res.* **41**: 66–97.
  65. Gliss, C., O. Randel, H. Casalta, E. Sackmann, R. Zorn, and T. Bayerl. 1999. Anisotropic motion of cholesterol in oriented DPPC bilayers studied by quasielastic neutron scattering: the liquid-ordered phase. *Biophys. J.* **77**: 331–340.
  66. Nakatani, Y., M. Yamamoto, Y. Diyizou, W. Warnock, V. Dollé, W. Hahn, A. Milon, and G. Ourisson. 1996. Studies on the topography of biomembranes: regioselective photolabelling in vesicles with the tandem use of cholesterol and a photoactivable transmembrane phospholipidic probe. *Chem. Eur. J.* **2**: 129–138.
  67. Rodriguez-Agudo, D., S. Ren, P. B. Hylemon, K. Redford, R. Natarajan, A. Del Castillo, G. Gil, and W. M. Pandak. 2005. Human StarD5, a cytosolic StAR-related lipid binding protein. *J. Lipid Res.* **46**: 1615–1623.
  68. Lascombe, M. B., M. Ponchet, P. Venard, M. L. Milat, J. P. Blein, and T. Prange. 2002. The 1.45 Å resolution structure of the cryptogin-cholesterol complex: a close-up view of a sterol carrier protein (SCP) active site. *Acta Crystallogr. D Biol. Crystallogr.* **58**: 1442–1447.
  69. Im, Y. J., S. Raychaudhuri, W. A. Prinz, and J. H. Hurley. 2005. Structural mechanism for sterol sensing and transport by OSBP-related proteins. *Nature*. **437**: 154–158.
  70. Goodford, P. J. 1985. A computational procedure for determining energetically favorable binding sites on biologically important macromolecules. *J. Med. Chem.* **28**: 849–857.
  71. de Graaf, C., P. Pospisil, W. Pos, G. Folkers, and N. P. Vermeulen. 2005. Binding mode prediction of cytochrome p450 and thymidine kinase protein-ligand complexes by consideration of water and rescoring in automated docking. *J. Med. Chem.* **48**: 2308–2318.
  72. Fornabaio, M., F. Spyraakis, A. Mozzarelli, P. Cozzini, D. J. Abraham, and G. E. Kellogg. 2004. Simple, intuitive calculations of free energy of binding for protein-ligand complexes. III. The free energy contribution of structural water molecules in HIV-1 protease complexes. *J. Med. Chem.* **47**: 4507–4516.
  73. Palomer, A., J. J. Perez, S. Navea, O. Llorens, J. Pascual, L. Garcia, and D. Mauleon. 2000. Modeling cyclooxygenase inhibition. Implication of active site hydration on the selectivity of ketoprofen analogues. *J. Med. Chem.* **43**: 2280–2284.
  74. Mathieu, A. P., A. Fleury, L. Ducharme, P. Lavigne, and J. G. LeHoux. 2002. Insights into steroidogenic acute regulatory protein (StAR)-dependent cholesterol transfer in mitochondria: evidence from molecular modeling and structure-based thermodynamics supporting the existence of partially unfolded states of StAR. *J. Mol. Endocrinol.* **29**: 327–345.
  75. Fleury, A., A. P. Mathieu, L. Ducharme, D. B. Hales, and J. G. LeHoux. 2004. Phosphorylation and function of the hamster adrenal steroidogenic acute regulatory protein (StAR). *J. Steroid Biochem. Mol. Biol.* **91**: 259–271.
  76. Kallen, J., J. M. Schlaeppli, F. Bitsch, I. Delhon, and B. Fournier. 2004. Crystal structure of the human RORalpha ligand binding domain in complex with cholesterol sulfate at 2.2 Å. *J. Biol. Chem.* **279**: 14033–14038.
  77. Feng, L., W. W. Chan, S. L. Roderick, and D. E. Cohen. 2000. High-level expression and mutagenesis of recombinant human phosphatidylcholine transfer protein using a synthetic gene: evidence for a C-terminal membrane binding domain. *Biochemistry*. **39**: 15399–15409.
  78. Bose, H. S., R. M. Whittal, M. A. Baldwin, and W. L. Miller. 1999. The active form of the steroidogenic acute regulatory protein, StAR, appears to be a molten globule. *Proc. Natl. Acad. Sci. USA*. **96**: 7250–7255.
  79. Baker, B. Y., D. C. Yaworsky, and W. L. Miller. 2005. A pH-dependent molten globule transition is required for activity of the steroidogenic acute regulatory protein, StAR. *J. Biol. Chem.* **280**: 41753–41760.
  80. Bose, H. S., M. A. Baldwin, and W. L. Miller. 2000. Evidence that StAR and MLN64 act on the outer mitochondrial membrane as molten globules. *Endocr. Res.* **26**: 629–637.
  81. Bose, H. S., R. M. Whittal, M. C. Huang, M. A. Baldwin, and W. L. Miller. 2000. N-218 MLN64, a protein with StAR-like steroidogenic activity, is folded and cleaved similarly to StAR. *Biochemistry*. **39**: 11722–11731.
  82. Christensen, K., H. S. Bose, F. M. Harris, W. L. Miller, and J. D. Bell. 2001. Binding of steroidogenic acute regulatory protein to synthetic membranes suggests an active molten globule. *J. Biol. Chem.* **276**: 17044–17051.
  83. Song, M., H. Shao, A. Mujeeb, T. L. James, and W. L. Miller. 2001. Molten-globule structure and membrane binding of the N-terminal protease-resistant domain (63–193) of the steroidogenic acute regulatory protein (StAR). *Biochem. J.* **356**: 151–158.
  84. Mathieu, A. P., P. Lavigne, and J. G. LeHoux. 2002. Molecular modeling and structure-based thermodynamic analysis of the StAR protein. *Endocr. Res.* **28**: 419–423.
  85. van Tiel, C. M., A. Schouten, G. T. Snoek, P. Gros, and K. W. Wirtz. 2002. The structure of phosphatidylinositol transfer protein alpha reveals sites for phospholipid binding and membrane association with major implications for its function. *FEBS Lett.* **531**: 69–73.
  86. Mason, J. M., M. J. Cliff, R. B. Sessions, and A. R. Clarke. 2005. Low energy pathways and non-native interactions: the influence of artificial disulfide bridges on the mechanism of folding. *J. Biol. Chem.* **280**: 40494–40499.
  87. Banci, L., I. Bertini, F. Cantini, N. D'Amelio, and E. Gaggelli. 2006. Human sod1 before harboring the catalytic metal: solution structure of copper depleted, disulfide reduced form. *J. Biol. Chem.* **281**: 2333–2337.

88. Choi, J., S. Choi, J. Choi, M. K. Cha, I. H. Kim, and W. Shin. 2003. Crystal structure of *Escherichia coli* thiol peroxidase in the oxidized state: insights into intramolecular disulfide formation and substrate binding in atypical 2-Cys peroxiredoxins. *J. Biol. Chem.* **278**: 49478–49486.
89. Jacobson, R. H., M. Matsumura, H. R. Faber, and B. W. Matthews. 1992. Structure of a stabilizing disulfide bridge mutant that closes the active-site cleft of T4 lysozyme. *Protein Sci.* **1**: 46–57.
90. Watari, H., F. Arakane, C. Moog-Lutz, C. B. Kallen, C. Tomasetto, G. L. Gerton, M. C. Rio, M. E. Baker, and J. F. Strauss, 3rd. 1997. MLN64 contains a domain with homology to the steroidogenic acute regulatory protein (Star) that stimulates steroidogenesis. *Proc. Natl. Acad. Sci. USA.* **94**: 8462–8467.
91. Routt, S. M., and V. A. Bankaitis. 2004. Biological functions of phosphatidylinositol transfer proteins. *Biochem. Cell Biol.* **82**: 254–262.
92. Vordtriede, P. B., C. N. Doan, J. M. Tremblay, G. M. Helmkamp, Jr., and M. D. Yoder. 2005. Structure of PITPbeta in complex with phosphatidylcholine: comparison of structure and lipid transfer to other PITP isoforms. *Biochemistry.* **44**: 14760–14771.
93. Friedland, N., H. L. Liou, P. Lobel, and A. M. Stock. 2003. Structure of a cholesterol-binding protein deficient in Niemann-Pick type C2 disease. *Proc. Natl. Acad. Sci. USA.* **100**: 2512–2517.
94. Dyer, D. H., S. Lovell, J. B. Thoden, H. M. Holden, I. Rayment, and Q. Lan. 2003. The structural determination of an insect sterol carrier protein-2 with a ligand-bound C16 fatty acid at 1.35-Å resolution. *J. Biol. Chem.* **278**: 39085–39091.
95. Breiteneder, H., and C. Mills. 2005. Nonspecific lipid-transfer proteins in plant foods and pollens: an important allergen class. *Curr. Opin. Allergy Clin. Immunol.* **5**: 275–279.
96. Wang, Z., W. Xie, F. Chi, and C. Li. 2005. Identification of non-specific lipid transfer protein-1 as a calmodulin-binding protein in *Arabidopsis*. *FEBS Lett.* **579**: 1683–1687.
97. Cheng, C. S., D. Samuel, Y. J. Liu, J. C. Shyu, S. M. Lai, K. F. Lin, and P. C. Lyu. 2004. Binding mechanism of nonspecific lipid transfer proteins and their role in plant defense. *Biochemistry.* **43**: 13628–13636.
98. Boissy, G., M. O'Donohue, O. Gaudemer, V. Perez, J. C. Pernollet, and S. Brunie. 1999. The 2.1 Å structure of an elicitor-ergosterol complex: a recent addition to the sterol carrier protein family. *Protein Sci.* **8**: 1191–1199.
99. Fefe, S., S. Bouaziz, J. C. Huet, J. C. Pernollet, and E. Guittet. 1997. Three-dimensional solution structure of beta cryptogin, a beta elicitor secreted by a phytopathogenic fungus *Phytophthora cryptogea*. *Protein Sci.* **6**: 2279–2284.
100. Boissy, G., E. de la Fortelle, R. Kahn, J. C. Huet, G. Bricogne, J. C. Pernollet, and S. Brunie. 1996. Crystal structure of a fungal elicitor secreted by *Phytophthora cryptogea*, a member of a novel class of plant necrotic proteins. *Structure.* **4**: 1429–1439.
101. Chen, J. C., L. J. Miercke, J. Krucinski, J. R. Starr, G. Saenz, X. Wang, C. A. Spilburg, L. G. Lange, J. L. Ellsworth, and R. M. Stroud. 1998. Structure of bovine pancreatic cholesterol esterase at 1.6 Å: novel structural features involved in lipase activation. *Biochemistry.* **37**: 5107–5117.
102. Yue, Q. K., I. J. Kass, N. S. Sampson, and A. Vrielink. 1999. Crystal structure determination of cholesterol oxidase from *Streptomyces* and structural characterization of key active site mutants. *Biochemistry.* **38**: 4277–4286.
103. Glatz, J. F., and J. Storch. 2001. Unravelling the significance of cellular fatty acid-binding proteins. *Curr. Opin. Lipidol.* **12**: 267–274.
104. Humphrey, W., A. Dalke, and K. Schulten. 1996. VMD: visual molecular dynamics. *J. Mol. Graph.* **14**: 33–38.
105. Heinig, M., and D. Frishman. 2004. STRIDE: a web server for secondary structure assignment from known atomic coordinates of proteins. *Nucleic Acids Res.* **32**: W500–W502.
106. Frishman, D., and P. Argos. 1995. Knowledge-based protein secondary structure assignment. *Proteins.* **23**: 566–579.